Petrogenesis and Geochemical Halos of the Amphibolite Facies, Lower Proterozoic, Kerry Road Volcanogenic Massive Sulfide Deposit, Loch Maree Group, Gairloch, NW Scotland.

Drummond[1,2,*], D.A. (drewdrummond59@gmail.com),

Cloutier[1,3], J., Boyce[2], A.J., Prave[1] A.R.

[1]School of Earth and Environmental Sciences, University of St Andrews, Irvine Building, KY16 9AL

[2]Scottish Universities Environmental Research Centre, Rankine Avenue, East Kilbride, Glasgow G75 0QF.

[3]Centre for Ore Deposit and Earth Sciences, University of Tasmania, Private Bag 79, Hobart, Tasmania, Australia

* Corresponding author

Abstract

The Palaeoproterozoic Kerry Road deposit is one of the oldest examples of volcanogenic massive sulfide (VMS) mineralization. This small VMS deposit (~500,000 tons grading at 1.2% Cu, 3.5% Zn) is hosted in amphibolite facies mafic-siliciclastic units of the c. 2.0 Ga Loch Maree Group, Scotland. Sulfide mineralization consists of pyrite and pyrrhotite with subordinate chalcopyrite and sphalerite, occurring in disseminated, vein and semi-massive to massive textures.

The deposit was highly deformed and metamorphosed during the c. 1.8–1.7 Ga Laxfordian Orogeny. Textural relationships of deformed sulfide minerals, related to early Laxfordian deformation (D1/D2), indicate initial high pressure-low temperature (100 MPa, 150ºC) conditions before reaching peak amphibolite facies metamorphism, as evident from pyrrhotite crossing the brittle/ductile transition prior to chalcopyrite. Late Laxfordian deformation (D3/D4) is marked by local retrograde greenschist facies at low pressure and temperature (<1.2MPa, <200°C), recorded by late red sphalerite remobilization. $\delta^{34}S$ values from all sulfide minerals have a homogeneous mean of 0.8 ± 0.7 ‰ (n=21), consistent with interaction of hydrothermal fluids in the host oceanic basalt-island arc setting envisaged for deposition of the Loch Maree Group.

Microprobe analyses of amphiboles record evidence of the original alteration halo associated with the Kerry Road deposit, with a systematic Mg- and Si- enrichment from ferrotschermakite (~150 m) to Mg-hornblende (~90 m) to actinolite (0 m) on approach to the VMS deposit. Furthermore, whole rock geochemistry records a progressive enrichment in Si, Cu, Co, and S, and depletion in Al, Ti, V, Cr, Y and Zr with proximity to the VMS system. These elemental trends, together with amphibole geochemistry, are potentially useful

exploration vectors to VMS mineralization in the Loch Maree Group, and in similar highly deformed and metamorphosed terranes elsewhere.

Key words: Kerry Road Deposit, Volcanogenic Massive Sulfide, Lewisian Complex, Alteration, S isotopes, sulfide deformation.

Introduction

VMS deposits form within extensional geodynamic regimes such as mid-ocean ridges, back-arc basins, and intraoceanic arc rifts (e.g., Swinden, 1991; Piercey, 2010, 2011; Hannington, 2014). Their formation is generally followed by deformation during accretionary tectonics that results in variable uplift, basin inversion, compressional deformation, and metamorphism of the sequence(s) hosting the massive sulfide lens(es) (e.g., McClay, 1995; Nelson, 1997). Deformation of VMS deposits is associated with strong rheological differences between the massive sulfide lenses and the more competent silicate-rich host rocks which commonly lead to significant remobilization of the sulfides (Cox, 1987; Marshall and Gilligan, 1987, 1989, 1993). Mosier *et al.* (2009) in their VMS deposit compilation (n=819) observed that only 3% of VMS deposits are hosted in unmetamorphosed rocks. In contrast, 8.5% are hosted in sub-greenschist facies, 62% are hosted in greenschist facies, 11% are hosted in amphibolite facies, 0.5% are hosted in granulite facies and 2% are hosted in blueschist/eclogite facies. In metamorphosed deposits, the primary alteration mineral assemblage changes to aluminous minerals (garnet, chloritoid, staurolite, kyanite/andalusite/sillimanite and cordierite), orthorhombic Mg-Fe-Mn amphiboles and gahnite (zincian spinel) (e.g., Nesbitt and Kelly, 1980; Corriveau and Spry, 2014; Hollis et al., 2019). The final metamorphic assemblage depends on the peak metamorphic grade and the original composition of the host rock and alteration zone. To date, most studies on metamorphosed VMS deposits focused on mineralization hosted in metasedimentary and felsic volcanic/volcaniclastic rocks (e.g., Nesbitt and Kelly, 1980; Barrett *et al.*, 2005; Duuring *et al.*, 2016; Mathieu *et al.*, 2016; Hollis et al., 2019). It is expected that VMS deposits hosted in metamafic rocks would contain a different mineral assemblage due to their higher abundance of Mg, Fe and Ca. This study investigates the chemical composition of

amphibole at the metamafic-hosted Kerry Road VMS deposit. The deposit is located in the Palaeoproterozoic (~2.0 Ga) Loch Maree Group (LMG) of the Lewisian Complex near Gairloch, NW Scotland (Fig. 1). It was discovered by Consolidated Gold Fields Ltd in 1978 on the basis of geological similarities to Archean to Proterozoic VMS-hosting belts in Canada and Scandinavia (Jones *et al*., 1987). The company drilled 87 cores in the Gairloch area, totaling 9189 m, and, although current outlined resources are sub-economic, it has repeatedly attracted exploration interest in Scotland (Jones *et al*., 1987; Coates *et al*., 1997; Colman and Cooper, 2000).

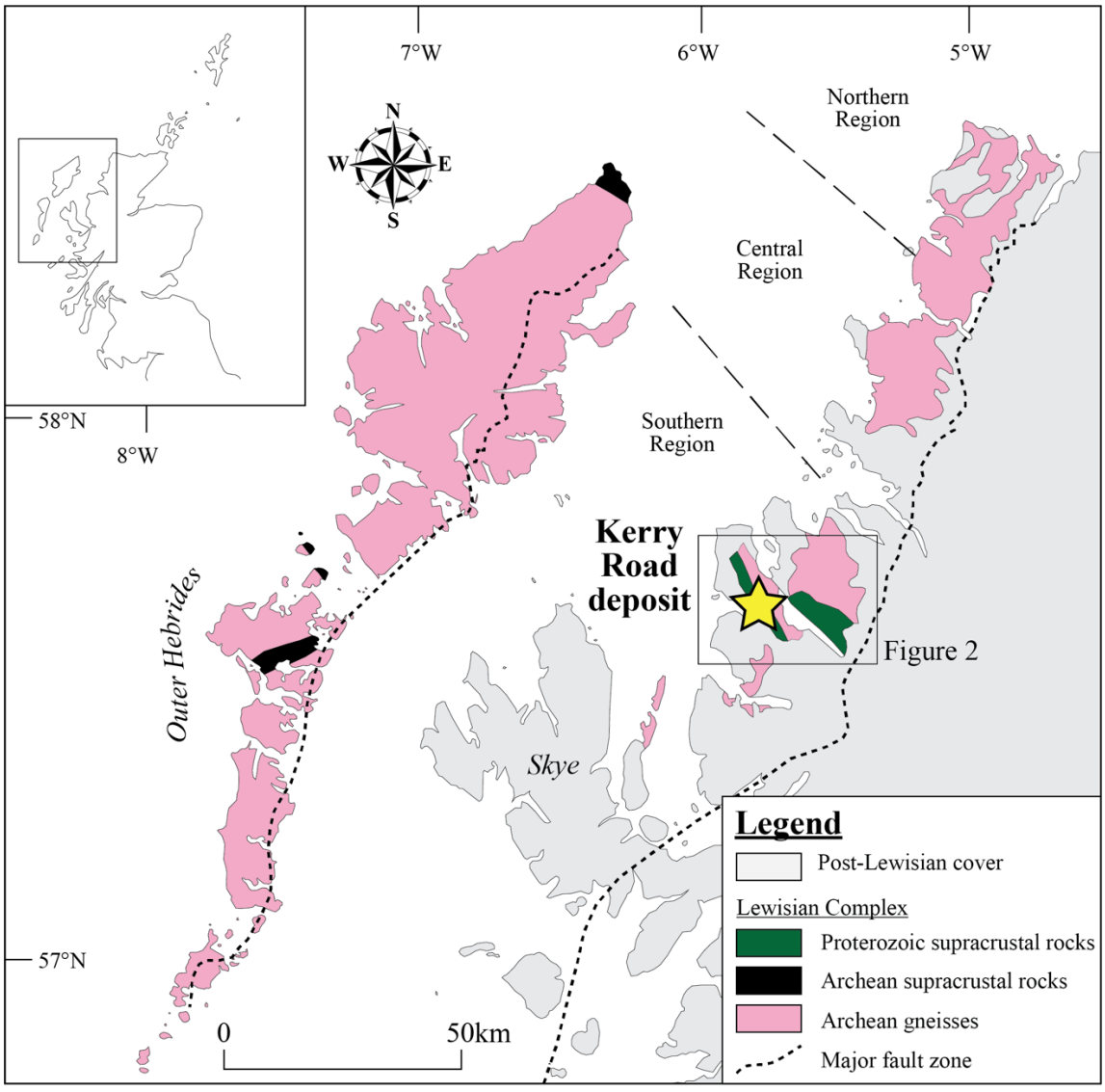

Figure 1. Simplified geological map of NW Scotland (modified from Coates et al., 1997).

The LMG has been studied extensively, particularly its structural framework (Peach et al., 1907; Park, 1964; Bhattacharjee, 1968; Park *et al*., 1987, 2001; Droop *et al*., 1999) and tectonic origin (Park *et al*., 2001). Far fewer studies have focused on VMS mineralization in the LMG and their utility in enhancing understanding of the regional geology (Jones *et al*., 1987; Colman and Cooper, 2000). Here we document the mineralogy, texture, deformation and sulfur isotope composition of the Kerry Road VMS deposit and surrounding rocks to evaluate their potential as exploration proxies within amphibolite facies metamafic volcanic sequences.

Regional Geology

Stratigraphy and Lithologies

The Lewisian Complex of NW Scotland consists mostly of Archean to early Proterozoic amphibolite to granulite facies metaigneous and subordinate metasedimentary rocks that experienced polyphase deformation (Davies 1978; Coward, 1990; Park *et al.*, 2001). On mainland Scotland, it forms a c. 200-km-long belt that is divided into three regions, consisting of a Central Region of granulite facies, which is bounded to the north and south by regions marked by amphibolite facies rocks. The LMG is part of the Southern Region and consists of metasedimentary and tholeiitic metavolcanic rocks that underwent amphibolite facies metamorphism related to what is termed the Laxfordian Event of c. 1.8-1.7 Ga (Park, 1964; Johnson *et al*., 1987; Jones *et al*., 1987; Whitehouse *et al*., 1997; Park *et al*., 2001). Although the exact tectonic setting remains speculative, the generally accepted model is an accretionary-subduction complex of oceanic plateau basalts (or primitive arcs) and associated abyssal sediments sandwiched between two Archean continental blocks (Park *et al*., 2001; Wheeler *et al*., 2010).

98 The LMG is divided into the Gairloch Schist Belt (GSB, ~36 km^2), which host the Kerry
99 Road deposit, and the Loch Maree Schist Belt (~60 km^2) which are separated by the Loch
100 Maree Fault (Johnson *et al*., 1987). Both comprise broadly similar successions of tholeiitic
101 metavolcanics, metapelites, metapsammites and rare banded-iron formation (of both oxide and
102 silicate facies), calcitic-dolomitic marble, calc-schist and graphitic mica-schist (Johnson *et al*.,
103 1987; Droop *et al*., 1999). Thin (typically <0.5 m), discontinuous exhalative horizons
104 dominated by silicate and oxide facies are present locally between metavolcanics and
105 metasedimentary units (Coates *et al*. 1997). Geochemical proxies on metasedimentary rocks
106 (REE, LIL elements, and major and trace elements) indicate mixing between a dominant
107 continental source (Lewisian gneissic basement) and a subordinate mafic volcanic source
108 (Floyd *et al*. 1989).

109 The GSB is intruded by c. 1.98 Ga metagranitoids, are cross-cut by the c. 1.99 Ga
110 Scourie dykes, and detrital zircons from metapsammites have yielded c. 2.0 Ga U-Pb ages
111 (Park, 2001; Whitehouse *et al.*, 1997; Baker *et al*., 2019). When combined, these provide
112 narrow brackets on the timing of mineralization. All LMG rocks were metamorphosed to
113 amphibolite facies during the 1.8-1.7 Ga Laxfordian event in which four phases of deformation
114 are recognized (Droop *et al.* 1999; Park *et al.*, 2001). D1 and D2 were ductile deformation
115 events associated with prograde condition that resulted in peak amphibolite-facies P-T
116 conditions. Thermodynamic analyses for a suite of LMG rocks yield peak P-T conditions of
117 6.5 ± 1.5 kbar and 530 ± 20 °C (Droop *et al*., 1999). Droop *et al.* (1999) defined D1 as a WNW-
118 ESE stretching and D2 as deformation associated with top-to-NW thrusting culminating in
119 intense mylonitization. Park *et al.* (2001) argues that the early D1 and D2 fabrics are
120 undistinguishable except where uncommon F2 folds affect S1 foliation. They consider D1 and
121 D2 to be a composite a fabric related to progressive early Laxfordian deformation. D3 and D4
122 were associated with post peak metamorphism retrogressive events (Park, 1964; Bhattacharjee,

1968; Park *et al*., 1987; Shihe and Park, 1993; Droop *et al*., 1999). D3 is associated with recumbent folds on steeply dipping F2 folds (Droop *et al.,* 1999). Park *et al.* (2001) attributed the timing of D3 as coincident with the emplacement of the Tollie pegmatites at 1.7 Ga, at low amphibolite- to greenschist-facies conditions. D4 is associated with small-scale (cm – m in amplitude), open and chevron steeply plunging folds with deforming the S1/S2 and S3 fabrics (Park, 1964; Bhattacharjee, 1968; Park *et al.*, 1987; Park *et al.*, 2001). D4 occurred in more localized narrow belts at sub-greenschist facies and is typically associated with narrow belts of cataclasis (Park *et al.*, 2001).

Geology of the Kerry Road VMS deposit

The first detailed description of the LMG massive sulfide mineralized lenses was by Jones *et al*. (1987) who identified two main occurrences. The North Sidmean Mor lens consists of iron sulfides with subordinate copper sulfides near the top of North Sidhean Mor and is traceable intermittently over 6 km. The other is the Kerry Road lens (another small satellite deposit, the Teangadh Bhuidhe Mhor deposit, is located nearby), which averages 4 m in thickness and extends for 580 m from Loch Bad an Sgalaig to Flowerdale Mains (Fig. 2; Williams *et al*., 1985; Coates *et al*., 1997). The Kerry Road deposit is estimated at 500,000 t at 1% Cu, 0.5% Zn and 1 g/t Au (Colman and Cooper, 2000) with base- and precious-metal massive sulfide mineralization hosted in quartz-carbonate schist and categorized as a mafic-siliciclastic or Besshi-type VMS deposit (Jones *et al*., 1987). The mineralization is fine-grained, commonly banded on mm-scales and displays massive, stringer and disseminated textures. Pyrrhotite and pyrite are the dominant sulfide minerals and total sulfides typically account for 15-20% of the rock. Other sulfides are present in subordinate amounts and include (in decreasing abundance) chalcopyrite, sphalerite, marcasite and galena. Rare native gold and magnetite are also present (Jones *et al*., 1987).

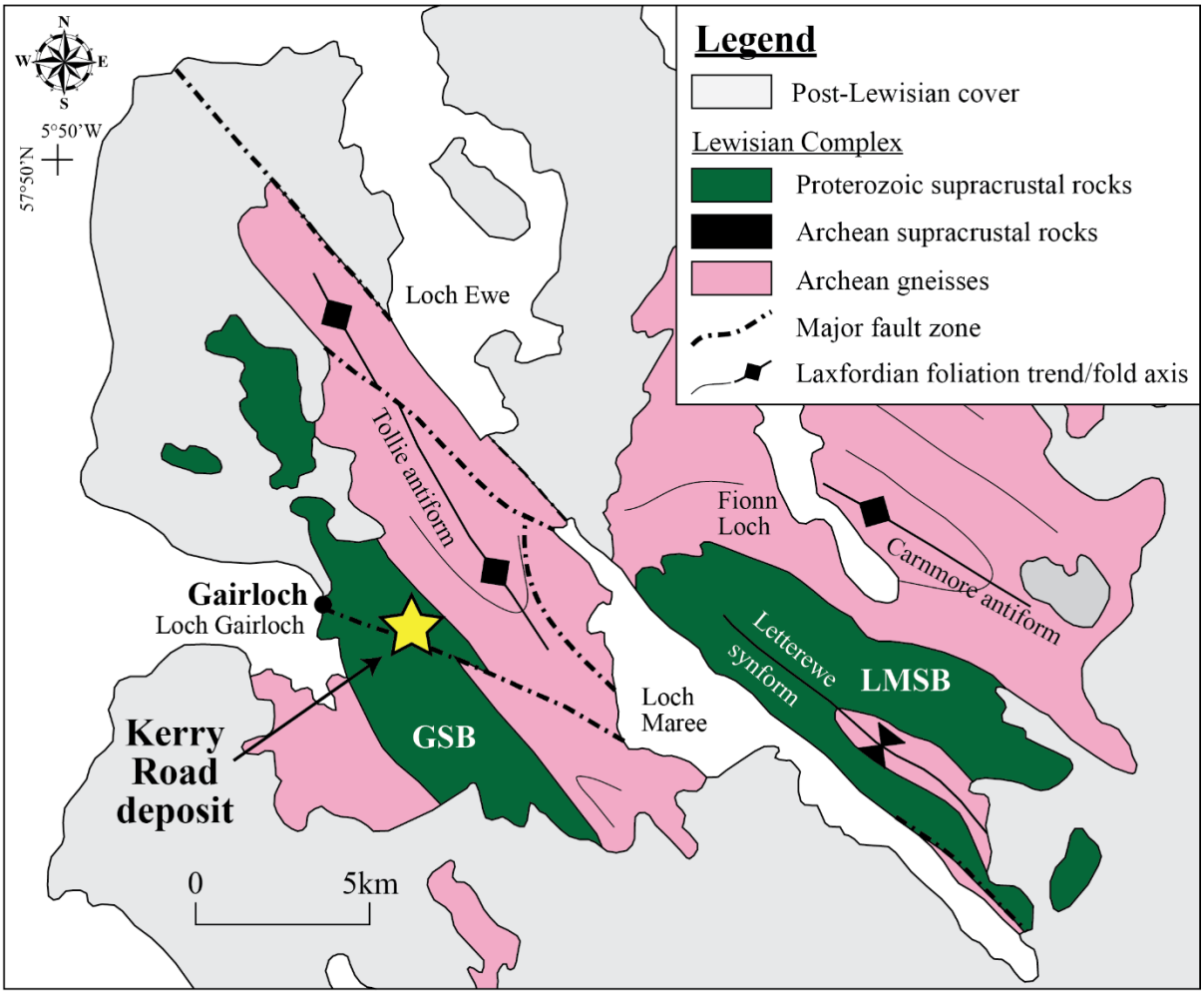

Figure 2. Simplified geological map of the Gairloch region (modified from Park et al., 1987, 2001). Also shown is the position of the Kerry Road deposit (star). GSB: Gairloch Schist Belt; LMSB: Loch Maree Schist Belt.

147

148 # Methodology

149 ## Field and Drill Core Analysis

150 Detailed mapping at a scale of 1:25,000 was undertaken at the Kerry Road deposit and
151 surrounding area (Fig. 3). Forty-one field samples were collected based on lithology and
152 mineralization. Furthermore, a total of ten diamond drill cores were logged in detail at the
153 British Geological Survey's Core Store, Keyworth, UK, and 38 core samples were collected.
154 From these, twelve samples were selected for polished thin-section petrography.

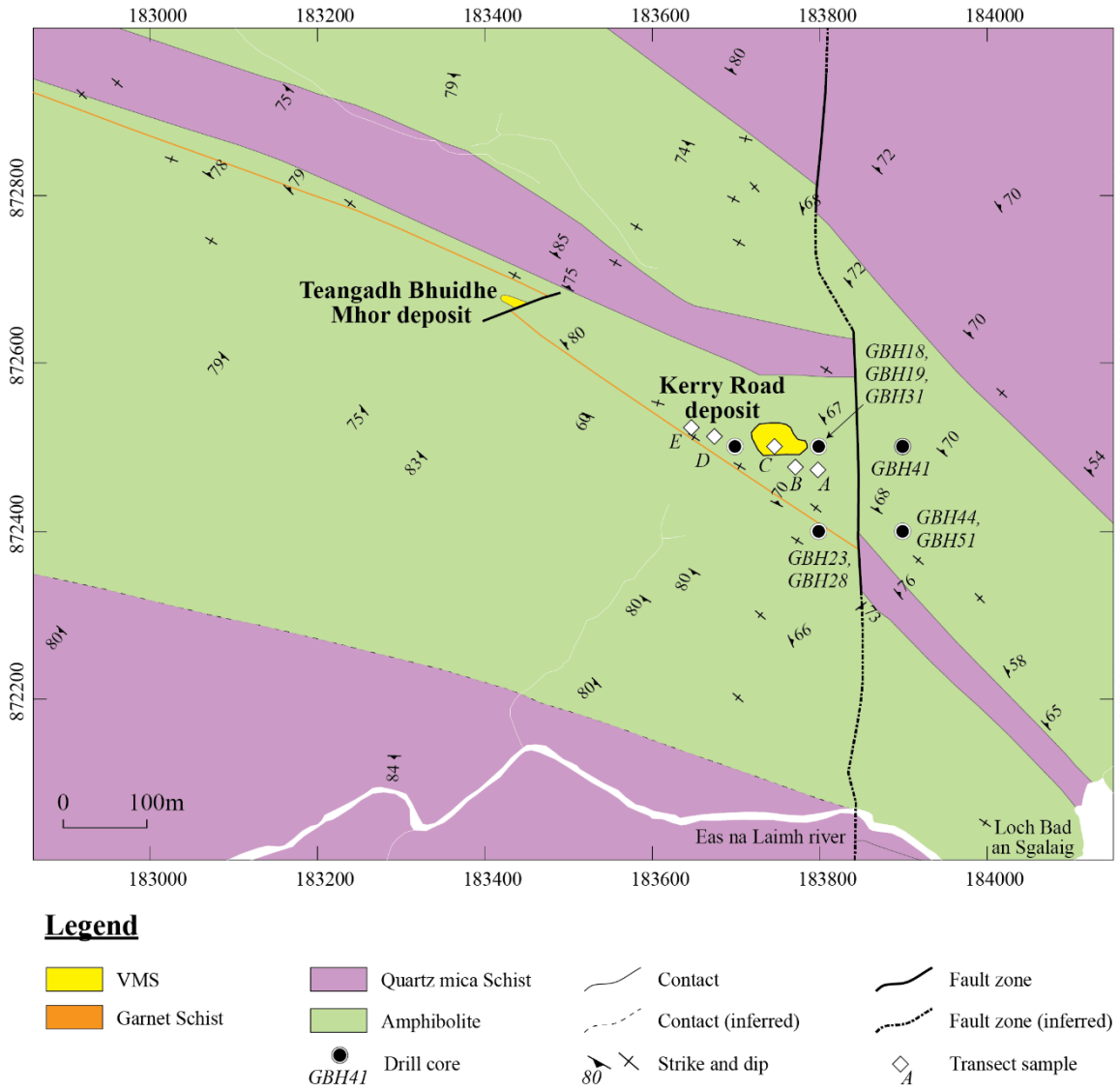

Figure 3: Geological map for the Kerry Road VMS deposit.

Electron Probe Micro-Analyzer

Four amphibole schist samples were selected from locations proximal and distal to the Kerry Road VMS deposit to assess amphibole compositional variation with distance to the deposit. Electron probe micro-analyzer (EPMA) analyses was carried out on a JEOL JXA-8600 Superprobe by the wavelength dispersive X-ray analysis method (WDS) at the University of St Andrews using conventional carbon coated polished sections (60-100 µm). Operating conditions were: 15 kv accelerating voltage, 20 nano-amperes (nA) beam current using a ~1µm

beam diameter to gain precise and accurate composition measurements of individual amphibole crystal cores and rims. Counting times were 20 s on peak, and background measurements were 10 s on each side of the analyzed peak. Background positions were carefully selected to avoid instances of peak overlap. Elements measured were Na, Mg, Al, Si, K, Ca, Ti, Mn and Fe. Standards used were Wollastonite (Si, Ca), Rutile (Ti), Corundum (Al), Metal (Fe, Mn), Periclase (Mg), Albite (Na) and Orthoclase (K). Detection limits varied between 0.05 and 0.2% depending on the element.

X-ray Fluorescence

Five samples were taken every 20-30 m along a ~150 m transect, following the regional strike direction of the Kerry Road deposit (Fig. 3), in order to test for alteration footprint and assess the change in geochemistry associated with the VMS system. Eight samples were selected from drill core to assess geochemical changes across the deposit and to identify the protoliths and tectonic origins of the geological units. Fifty grams of weathering-free sample were crushed to a fine powder using a laboratory disc mill with a tungsten carbide grinding jar for 90 seconds. Pressed-powder pellets were prepared by mixing 8 g of sample powder with 12 drops of polyvinyl alcohol, pressing the mixture to a disc at 15 tons for 30 seconds, and drying overnight at 60 °C. Trace element concentrations for V, Cr, Co, Ni, Cu, Zn, As, Rb, Sr, Y, Zr, Nb, Mo, Ag, Cd, Sn, Ba, La, Ce, Pb, Th and U and semi-quantitative major element concentrations for Al, Si, P, S, K, Ca, Ti, Mn, Fe were obtained by irradiating the sample with high energy X-rays from a controlled X-ray tube using a SPECTRO® XEPOS HE at the University of St Andrews. The method uses fundamental calibration parameters using >20 internationally recognised (mainly silicate) certified reference materials (CRM).

Sulfur Isotope Analyses

Sulfides were prepared for conventional isotopic analyses by diamond micro-drilling techniques on 21 samples and analyzed by standard techniques at the Scottish Universities Environmental Research Centre (SUERC; Robinson and Kusakabe, 1975) in which SO_2 gas was liberated by combusting the sulfides (5-10 mg) with excess Cu_2O at 1075°C, *in vacuo*. Liberated gases were analyzed on a VG Isotech SIRA II mass spectrometer and standard corrections applied to raw $\delta^{66}SO_2$ values to produce true $\delta^{34}S$. The standards employed were the international standards NBS-123 and IAEA-S-3 , and the SUERC standard CP-1. Repeat analyses of these standards gave $\delta^{34}S$ values of +17.1‰, -32‰ and -4.6‰ respectively, with a standard error of ± 0.3‰ or better. Data are reported in $\delta^{34}S$ notation as per mil (‰) variations from the Vienna Cañon Diablo Troilite (V-CDT) standard.

Results

Stratigraphic Sequence

Detailed mapping of the Kerry Road region reveals that the main lithologies are quartz-mica schist, amphibolite, garnet schist and massive sulfide (Figs. 4, 5); contacts between these units are generally sharp. Laxfordian deformation has resulted in a dominant sub-vertical layer-parallel foliation.

Quartz-mica schist is dark grey to black semipelitic-siliceous unit with a uniform fine-grained texture (<1 mm; Fig. 4ab). It is composed of quartz, biotite, chlorite and muscovite that typically define the main foliation. Accessory minerals include pyrite, garnet and plagioclase. Localized folding can be observed in siliceous horizons. Quartz veins (0.5 mm - 10 cm) are

found parallel to as well as cross-cutting the foliation, suggesting multiple phases of quartz formation.

Amphibole schist is typically, dark green with amphibole porphyroblasts from 1 mm to 2 cm, coarse- to fine-grained quartz, medium- to fine-grained amphiboles and subordinate fine-grained chlorite that can become dominant locally (Fig. 4cd). Porphyroblasts of amphibole commonly displays a garbenschiefer texture in which porphyroblastic crystals of amphibole form stellate or sheaflike groups on the planes of foliation or schistosity. Outcrops commonly display at least two phases of foliated amphibole porphyroblasts suggesting several phases of growth/deformation. Folding is intense proximal to the Kerry Road deposit where crenulation cleavage is developed.

Garnet-amphibole schist is a 2 m thick unit that can be traced along strike from the VMS deposit for approximately 1 km. The unit has similar textures and modal abundances to the amphibole schist but with the addition of garnet (~15%; Fig. 4ef). Garnet is of almandine composition with weak zonation in some crystals and inclusions of quartz. It overprints amphibole with no evidence of shearing or pressure shadows, implying static crystallization. Amphibole crystals display a clear foliation and appear to overprint a matrix of fine chlorite and quartz with subordinate amphibole. Locally, chlorite overprints amphibole, suggesting a later greenschist facies overprint.

Sulfide mineralization at the Kerry Road deposit is exposed over a ~30 x ~20 m area. The mineralization is hosted in amphibolite and is highly weathered and oxidized at the surface with prominent secondary malachite and iron oxide forming a gossan. The deposit displays complex folding. Dominant sulfide mineralization exists as pyrite and pyrrhotite, with subordinate chalcopyrite and sphalerite (Fig. 5ab). Sulfides coexist with silicate and carbonate

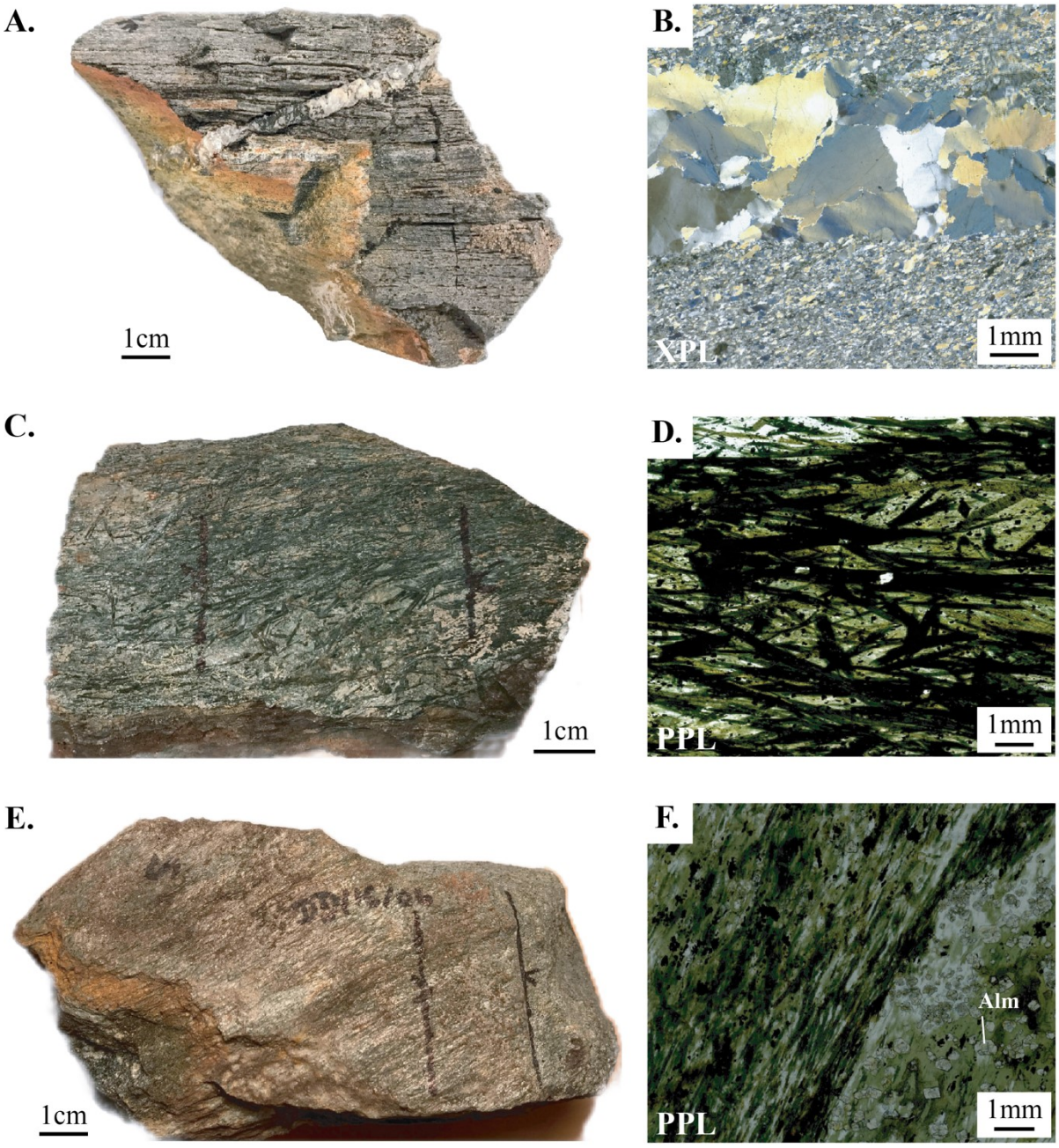

Figure 4: Examples of rock types in the Kerry Road field area and the associated petrographic analysis. A) Quartz-mica-schist sample DD/16/09, with quartz veins running parallel and cross-cutting the dominant foliation. Modal abundance is quartz (~81%), biotite (~10%), pyrite (~4%) muscovite (~4%), plagioclase (~1%). B) Thin section of sample DD/16/09, outlining the sheared foliation, and quartz veining cross-cutting quartz, biotite and chlorite matrix. C) Sample DD/16/04 displaying porphyroblastic amphiboles. D) Thin section of sample DD/16/04 wherein a sub-lineation defines the amphibole crystals. Microprobe analyses of these crystals identified them as ferrotschermakite. At least two phases of amphibole growth are suggested due to overlapping relationships. E) Sample DD/16/06 consisting of garnet-amphibole-schist with almandine garnets overprinting foliated amphibole. Mode for this sample consisted of amphibole (35%), quartz (25%), chlorite (20%), almandine (15%), iron oxide (5%). F) Thin section of sample DD/16/06 with almandine garnets overprinting sheared deformation fabric and displaying static growth suggesting their growth was late and thus continuation of amphibolite facies conditions even at the later stages of Laxfordian deformation. Note, though that almandine crystals show clear signs of retrogression to chlorite and quartz (greenschist facies assemblage).

230

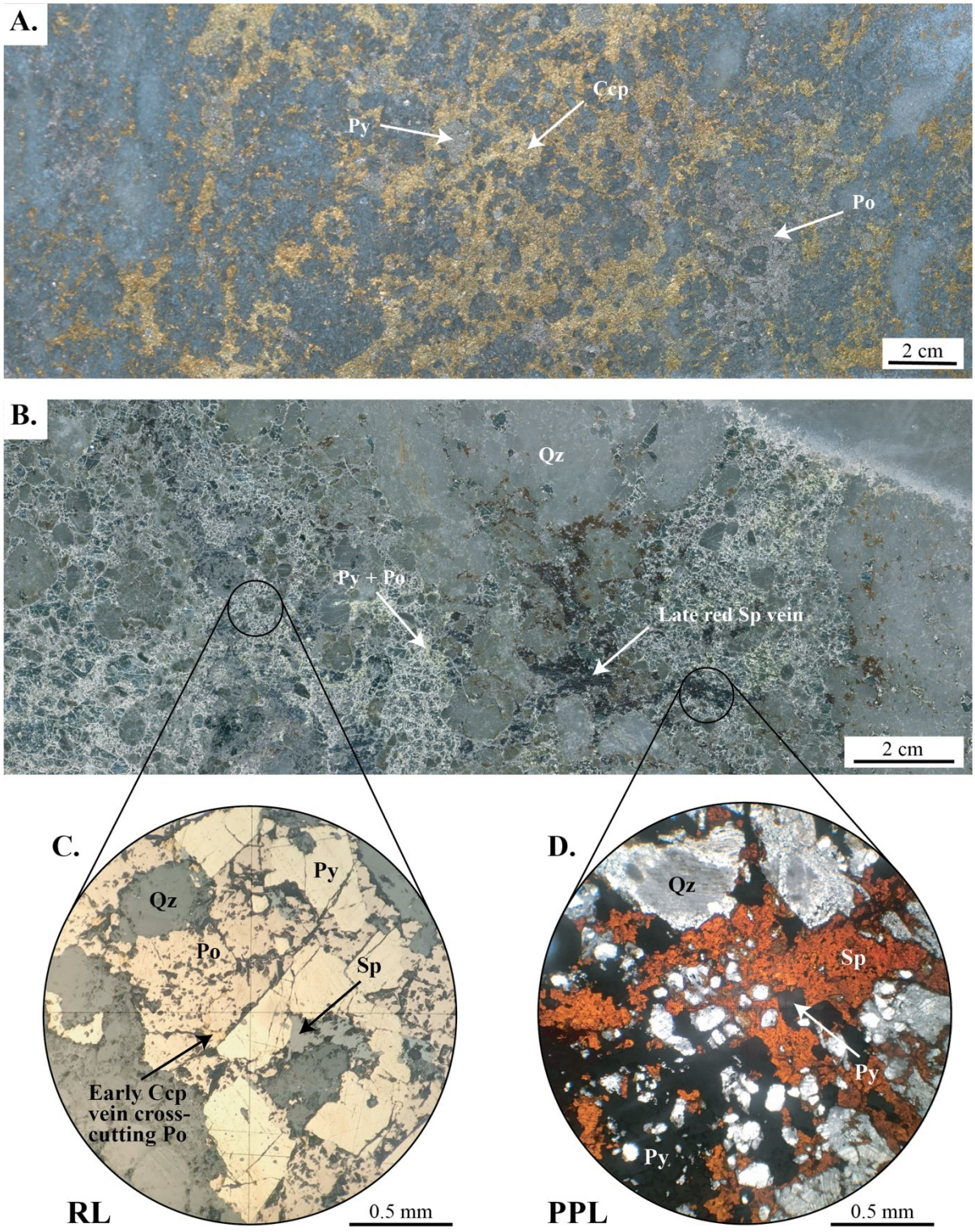

Figure 5: Photo of mineralized intervals at the Kerry Road deposit. A) Sample highlighting the common mineralogy and sulfide remobilization textures observed. Gangue includes quartz, ferroan dolomite and calcite (GBH18; 30m). (B) VMS sample 70033 from drill core GBH23 at a depth of 29.45-29.7 m. Both samples show a remobilization sequence wherein pyrrhotite crosses the brittle/ductile boundary first followed by chalcopyrite and sphalerite. Pyrite has not been remobilized and acted brittlely during deformation. Ccp= chalcopyrite, Py= pyrite, Po= pyrrhotite.

231

gangue such as quartz, chlorite, ferroan dolomite, calcite and amphibole. No systematic vertical or lateral zonation in base metal sulfides were observed.

Sulfide Remobilization and Textural Analyses

Textures identified in the Kerry Road deposit include disseminated (35%), vein (10%), and sub-massive/massive sulfide (55%) (Fig. 6a-d). Disseminated textures occur as discrete sulfide crystals hosted within a silicate matrix, whereas sulfide veins are typically chalcopyrite-bearing. Durchbewegung texture is common in sub-massive to massive sulfide regions (Fig. 6e). Durchbewegung texture, as defined by Marshall and Gilligan (1989), consists of a mixture of secondary tectonic origin composed of angular to rounded clasts of competent materials (e.g., silicates) within a matrix of predominantly less competent material (e.g., sulfides) where the competent clasts are generally contorted and disoriented.

Pyrrhotite, sphalerite and chalcopyrite do not display discrete individual grain boundaries resulting in crystals that cross-cut and fill fractures and interstitial spaces between gangue and pyrite crystals. Pyrite forms subhedral crystals that exhibit brittle behavior (Fig. 6b). Cross-cutting relationships show that pyrrhotite mobilized first followed by chalcopyrite and sphalerite (Fig. 5b). Locally, pyrite has been encased by remobilized chalcopyrite, pyrrhotite and sphalerite, indicating P-T conditions that allowed ductile remobilization into low pressure areas such as crystal fractures, grain boundaries and within interstitial spaces between gangue minerals. In some cases, the pyrite crystals have undergone mechanical reworking and are cataclastically deformed. Annealed pyrite textures were observed, which typically dominate at medium-high metamorphic grades (McClay and Ellis, 1983); this texture is marked by equant grains with triple junctions and straight grain boundaries.

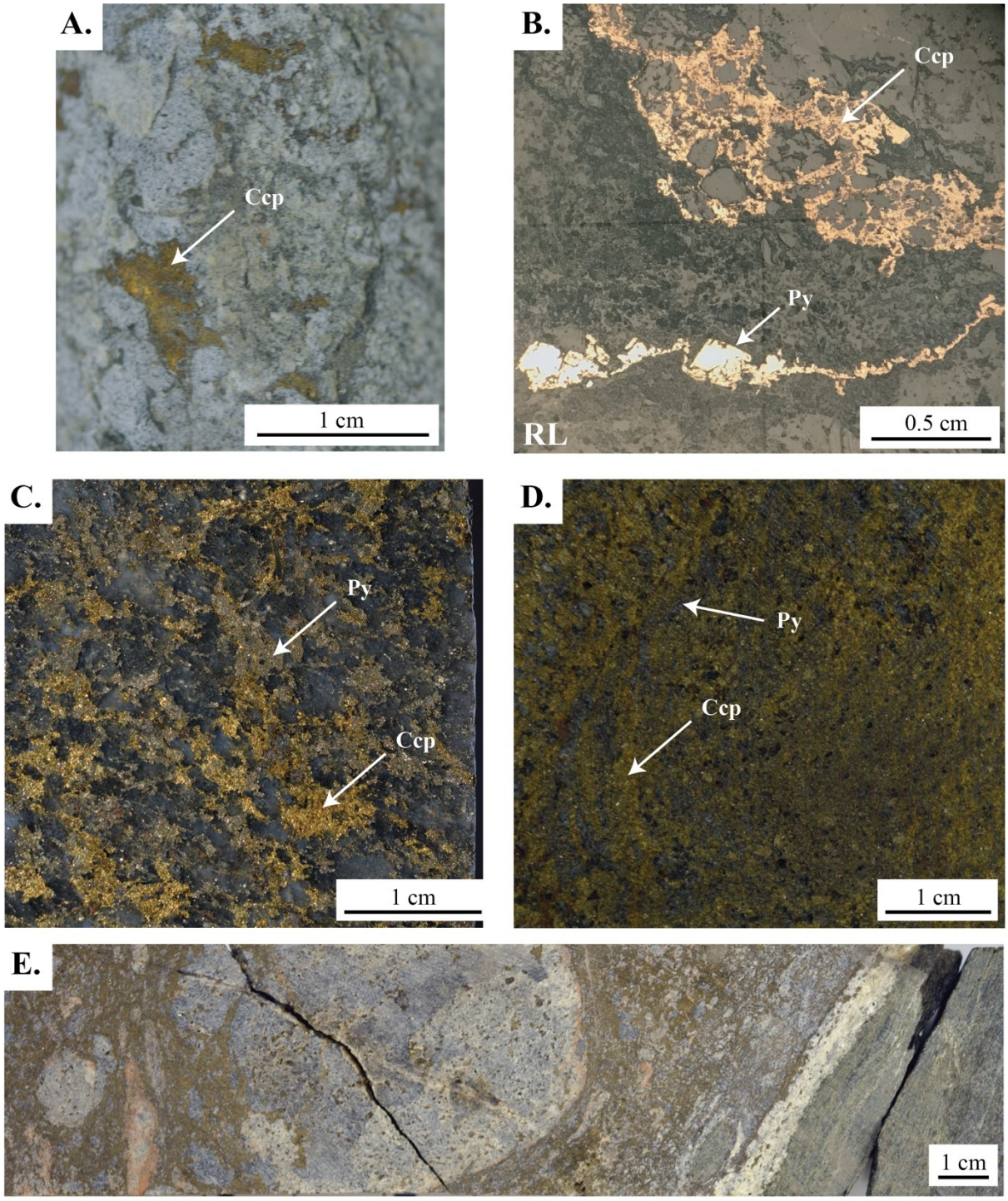

Figure 6: Photographs of the different sulfide mineralization texture. A) Disseminated mineralization showing isolated chalcopyrite aggregates in a matrix of silicates. Drill core GBH15, 20.5-22.5 m. B) Vein-type mineralization exploiting an ultramylonite horizon, displaying chalcopyrite veining and pyrite cubes. Veining engulfs euhedral pyrite and is not influenced by mylonitic shearing suggesting that remobilization continued to occur after peak mylonitic conditions. Drill core GBH31, 73.16-73.36 m. C) Sub-massive texture displaying both chalcopyrite and pyrrhotite mineralization. Drill core GBH41, 109.2-112 m. D) Massive texture with dominant chalcopyrite. Drill core GBH19, 25.3-27.2 m. E) Durchbewegung texture; defined as a mixture of secondary tectonic origin composed of angular to rounded clasts of one or more competent materials in a matrix of predominantly different incompetent material (in this case pyrrhotite). Significant clast rotation has occurred through deformation to form this round clast (Marshall and Gilligan, 1987). Note the calcite exploiting the contact between the VMS mineralization and the amphibole schist. Drill core GBH19, 33.0-33.4 m.

254

Whole Rock Geochemistry

Immobile elements such as Al, Ti, the high field strength elements (HFSE) and the REE (except Eu) are ideal to provide information on the primary petrochemical attributes of the host rocks in VMS systems (e.g., Large, 1977; Hannington, 2014; Cloutier *et al.*, 2017). However, caution must be used as some of these elements may become mobile (especially the LREE) during intense hydrothermal alteration (MacLean, 1988). At Kerry Road, the amphibolite samples falls within the basalt/andesite field of Pearce (1996) (Fig. 7a), the tholeiitic field of Ross and Bedard (2009) (Fig. 7b), the island arc tholeiite of Shervais (1982) (Fig. 7c) and within the post-Archean juvenile environment of Piercey (2009) (Fig. 7d).

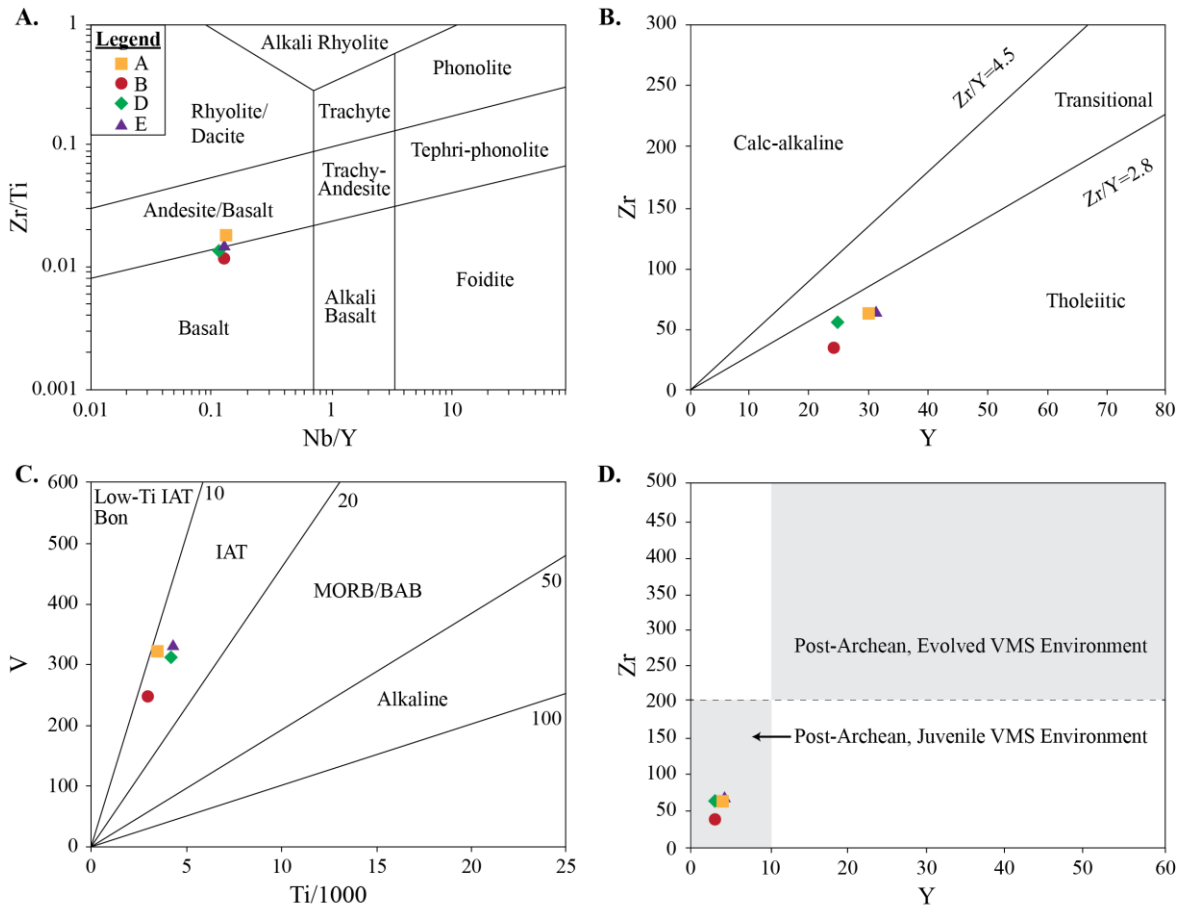

Figure 7: Immobile element discrimination diagrams for distal amphibolite surrounding the Kerry Road deposit (A) Zr/TiO2-Nb/Y diagram (Winchester and Floyd, 1977) with modified field boundaries of Pearce (1996). B) Zr-Y discriminating magma affinity with fields of Ross and Bedard (2009) (C) V-Ti/1000 diagram with field boundaries of Shervais (1982) for mafic rocks. (D) Zr-Nb diagram of Piercey (2009) discriminating juvenile environments from evolved environments. Low Ti-IAT Bon= low titanium-island-arc tholeiites and boninites, IAT=island-arc tholeiites, MORB/BAB= mid-ocean ridge basalts/back-arc basalts.

Mineralized samples throughout the deposit (n=9) vary between 14-30% S, 17-39% Fe, 0.3-3.8% Cu, 0.2-6.4% Zn, 8-594 ppm Pb and 450-1839 ppm Co (Table 1). These values are significantly higher than average values of 0.44% Cu and 0.42% Zn published by Jones *et al.* (1987). To test enrichment of elements in and near the ore zone, a transect of five samples across the deposit was designed and shows that the Kerry Road VMS lens is associated with enrichment in Si (x1.5), S (x33.3), Co (x17.6), and Cu (x7.6), and depletion in Al (x0.02), Ti (x0.01), V (x0.03), Cr (x0.03), Y (x0.1) and Zr (x0.17) (Fig. 8).

An isocon diagram shows that most element hosted in mineralized area are near the 1:1 line and have been conserved compared to the unmineralized amphibolite (Fig. 9). The diagram shows that the mineralization is associated with an increase of S, Pb, Co, Cu, Zn and depletion of Al, Ti. In general, these trends are in agreement with observed trend over the transect (Fig. 8). The main differences relate to the intensity of the changes and can be associated with the isocon diagram using averages of the samples compared to single samples for the transect. Elements such as V, Cr, Y and Zr will not incorporate into the sulfides and will be further diluted when massive sulfide is present (i.e., mass gain).

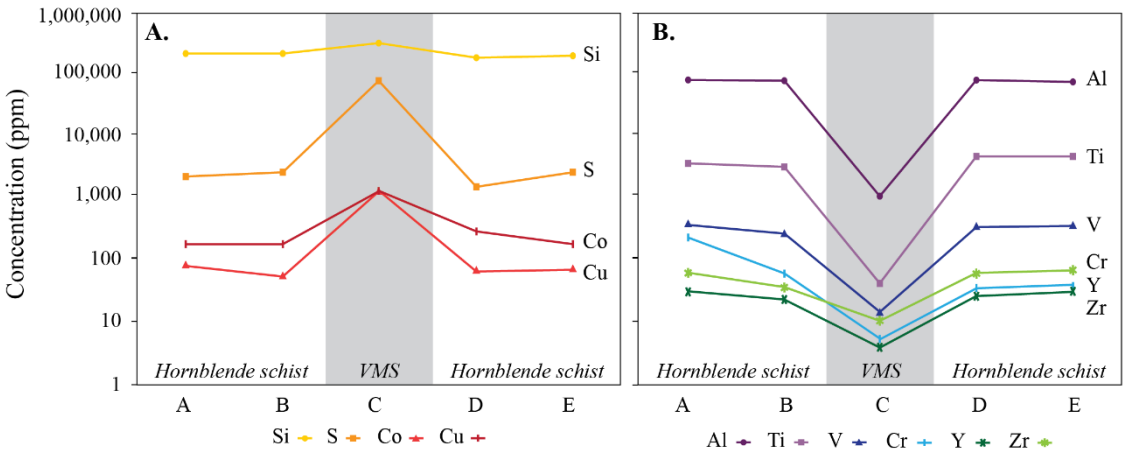

Figure 8: Major and trace element A) enrichment and B) depletion associated with whole-rock geochemical analysis along the Kerry Road deposit transect. Sample 2C is from the Kerry Road VMS deposit; other samples are all associated with amphibolite host rock.

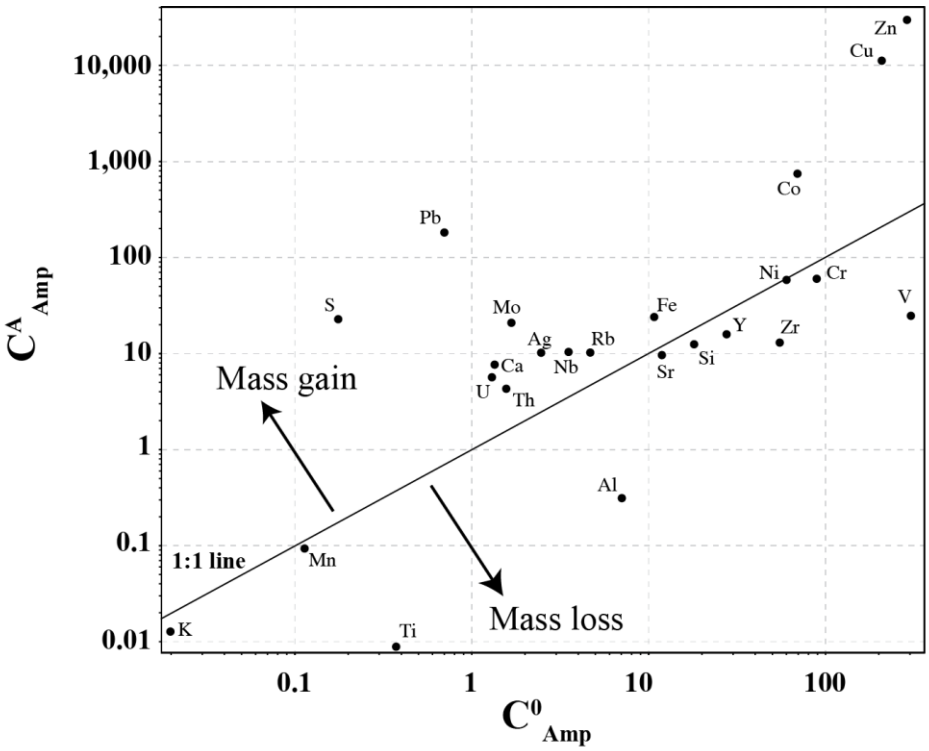

Figure 9: Isocon diagram (after Grant, 2005) illustrating the whole-rock chemical changes between unmineralized and mineralized amphibolite. Major elements are in wt% and trace elements in ppm.

282

283 **Amphibole chemistry**

284 Amphiboles were analysed to test for compositional changes with varying proximity to
285 the Kerry Road deposit (Fig. 10; Table 2). Samples DD.16.04 (~250 m) and 70060 (~150 m)
286 are distal and consist of ferrotschermakite ($Ca_{1.6}(Mg_{0.03},Fe_{2.44})Al_{2.6}Si_{5.93}O_{22}(OH)_2$), with
287 relatively low Mg and Si content compared to the proximal (~100 m) and mineralized sample.
288 Transect sample A is within ~100 m of the Kerry Road deposit and has a composition between
289 magnesiohornblende and actinolite, highlighting a transition towards more Si and Mg. Sample
290 70027 is associated with the mineralization and consist of actinolite with the highest Mg and
291 Si concentrations ($Ca_{1.7}(Mg_{3.9},Fe_{1.1}Si_{7.94}O_{22}(OH)_2$).

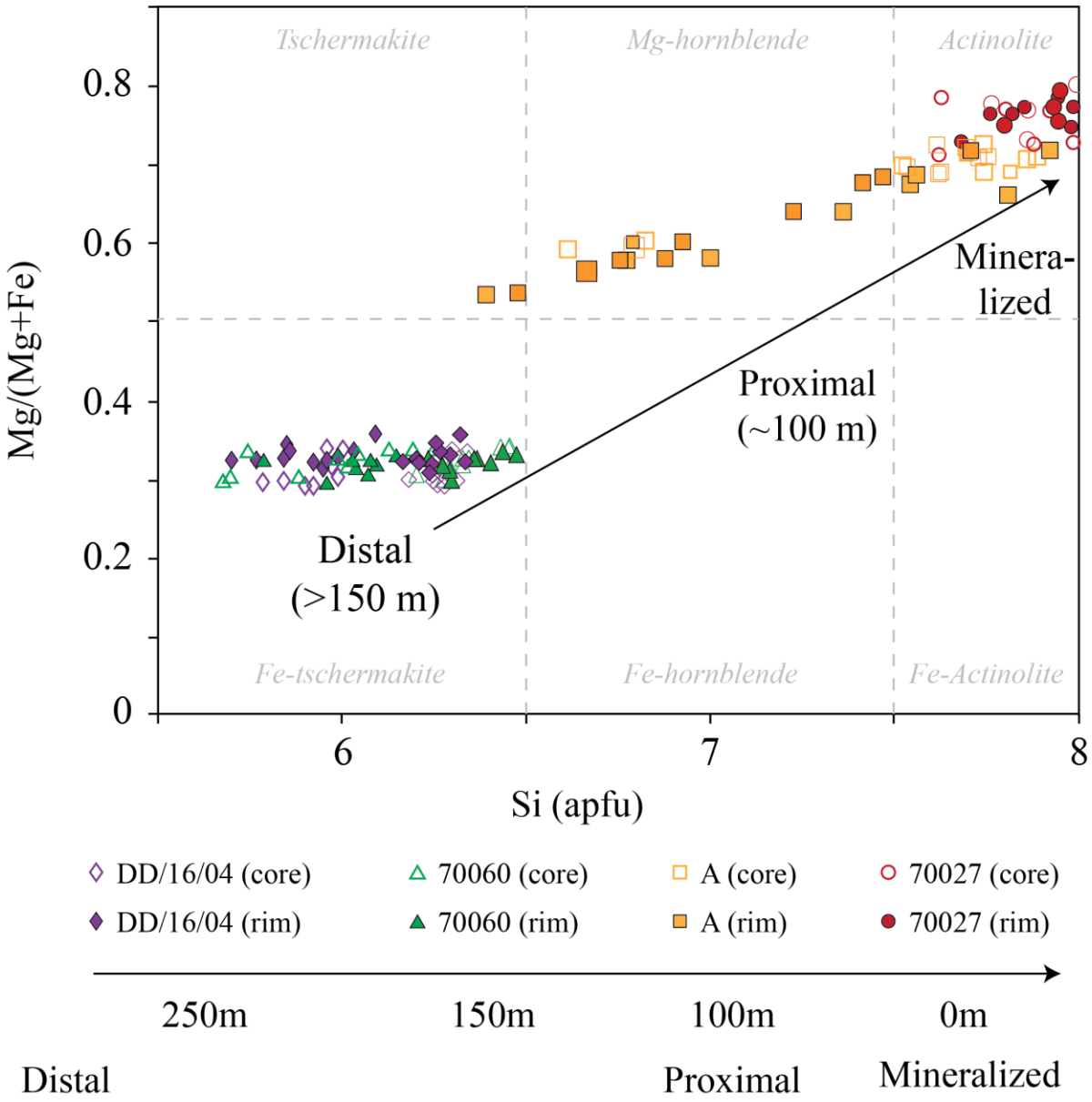

Figure 10: Chemistry of amphibole at the Kerry Road area derived from microprobe analyses. Amphibole chemistry changes from ferrotschermakite in distal samples (70060 and DD/16/04) to actinolite in proximal samples (1A and 70027). This change highlights a progressive enrichment in Si and Mg as the Kerry Road deposit is approached. Classification of calcic amphiboles fields modified from Leake et al.

Sulfur Isotope Analyses

Sulfur isotope analyses of pyrite, sphalerite and chalcopyrite from the mineralized samples are remarkably homogeneous and average $\delta^{34}S‰$ = 0.8 ‰ (±0.7 ‰) (n=21). Pyrrhotite (n=4) range between -0.5 and 1.1‰, pyrite (n=13) range between 0.7 and 2.1‰, and chalcopyrite range between 0.3 and 1.2‰ (Fig. 11; Table 3).

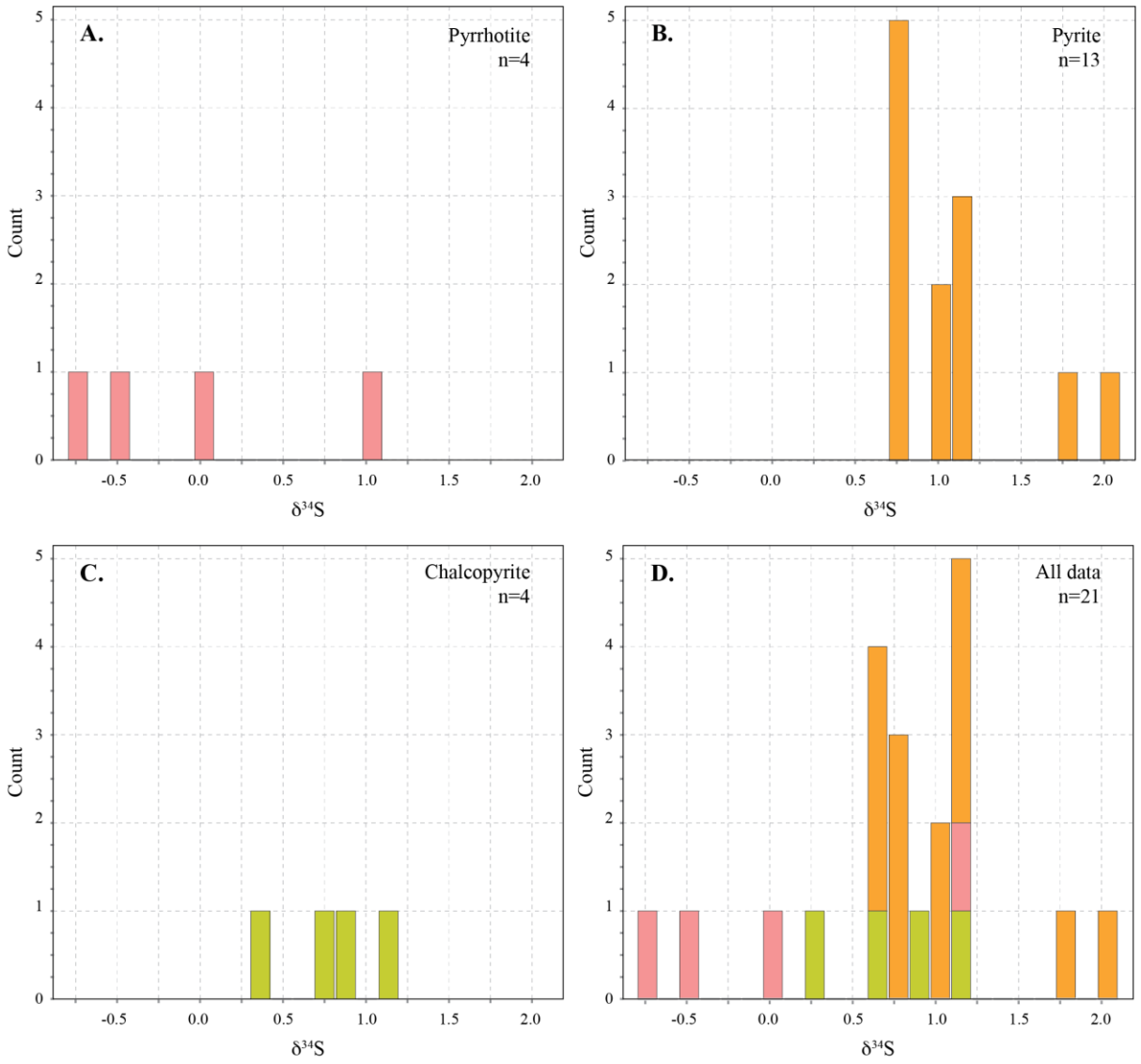

Figure 11: Sulfur isotope analysis (n=21) from the Kerry Road Deposit. The majority of the samples are near 0 ‰ and reflect a basaltic source for the sulfur found in the base metal sulfides.

Discussion

Tectonic setting of formation for the Kerry Road deposit

In the last twenty-five years, a classification scheme of VMS deposits has been developed based on host stratigraphic sequence and interpreted geodynamic setting (Barrie and Hannington, 1999; Piercey, 2010, 2011). In metamorphic terranes, the primary features of rocks are often obscured due to mineralogical changes but, in general, their chemical composition reflects that of their protolith. In such circumstances, trace element geochemistry

306 can be used to provide insights into the nature of the protolith and its tectonic setting (Vokes,
307 2000; Spry *et al.*, 2000; Cook and Marshall, 2004; Corriveau and Spry, 2014). The Kerry
308 Road deposit is characterized by amphibolite facies metamorphosed tholeiitic basalts and
309 metapsammite/pelite. This type of VMS deposit forms in tectonic environments associated
310 with oceanic island-arc or continental rift/back-arcs basins and is dominated by pelitic and
311 mafic lithologies (e.g., Franklin *et al*., 2005; Galley et al., 2007). Moreover, trace element
312 systematics of the metabasalts are compatible with a pre-Laxfordian submerged island arc
313 tholeiite interpretation (Fig. 7bc). This is supported by the tight distribution of $\delta^{34}S$ data,
314 averaging at 0.8 ‰, reflecting a homogenous sulfur source dominated by tholetiitic basalts
315 with $\delta^{34}S$ around 0‰ (Torssander, 1992). The primary signature appears to have been
316 preserved, on the hand specimen and deposit scale. A similar relationship was recorded in the
317 Norwegian Caledonide VMS systems, which have undergone similar metamorphism (Skauli
318 et al, 1992; Cook and Hoefs, 1997), and also preserved characteristics of the magmatic origin
319 of their host VMS. However, the homogeneity of the signal was likely "tightened" through
320 the deformation and metamorphism. Nonetheless, an alternative interpretation of the origin of
321 the S signature, is that this cluster might reflect Paleoproterozoic seawater with $\delta^{34}S$ between
322 15 and 25 ‰, as partial reduction of oxidized seawater to isotopically lighter H_2S results in
323 sulfides ~17 to 25‰ lighter than coexisting seawater sulphate (e.g., Ohmoto and Rye, 1979;
324 Seal, 2006; Cloutier *et al.*, 2015). However, this is unlikely as Blättler *et al.* (2018)
325 determined the $\delta^{34}S$ of seawater from a 2.0 Ga evaporite sequence to be between 5 and 7‰.
326 If the S-isotope composition of the LMG sulfides were derived from 2.0 Ga seawater their
327 $\delta^{34}S$ should be –10 to –20‰. Therefore, we conclude that the sulfides originated from the
328 tholeiitic basalts.

329

Deformation of the Kerry Road deposit

In the Kerry Road field area, Laxfordian D1/D2 defines penetrative sub-vertical foliation associated with prograde amphibolite facies metamorphism that is typically attributed to the collision of an oceanic plateau with a continental accretionary prism at c. 1.9 Ga (Park et al., 2001). In the Kerry Road area, this phase of deformation is recorded by the strong, steeply dipping NW-SE (~120°) foliation. This led to significant recrystallization and mechanical remobilization of pre-existing sulfide mineralization. Through cross-cutting relationships, pyrrhotite was observed to remobilize first, followed by chalcopyrite and finally sphalerite (Fig. 5b). Maximum peak metamorphic conditions were not high enough for pyrite to cross the brittle-ductile boundary as evidenced by its brittle deformation behavior (Fig. 12). The pyrrhotite-chalcopyrite relationship suggests that pressure crossed the 100 MPa mark before reaching 150°C (Marshall and Gilligan, 1987; Fig. 12), which is compatible with subduction tectonics P-T. However, the late remobilization of sphalerite does not fit the Barrovian-type sulfide remobilization sequence of Marshall and Gilligan (1987) wherein galena crosses the brittle ductile boundary first followed by sphalerite, pyrrhotite, chalcopyrite and pyrite (Fig. 12). This suggests that sphalerite was remobilized again under either D3 or D4 (or both) and that these late Laxfordian events did not reach pressures above 120 MPa (Po remobilization) and temperature above 200°C (Ccp remobilization), which is consistent with the established D3/D4 brittle retrogressive metamorphic events of Park *et al.* (2001).

Peak Laxfordian metamorphic conditions in the Kerry Road area are highlighted by the presence of index minerals such as amphibole, garnet and biotite. Two stages of amphibole growth were observed, correlating with D1/D2 fabrics. Many of the early amphibole porphyroblasts display a well-developed mineral elongation lineation that may

correspond with the L1 mineral lineation of Park *et al.* (2001). In places, amphiboles display intergranular shear movement, suggesting shearing post-peak metamorphism. Furthermore, zoned almandine garnets, cross-cut the main foliation defined by the amphiboles, and do not display concentric rings or spiral trails inclusions suggesting their growth was late and that peak metamorphic conditions were stable enough to allow static growth of garnet. Late retrogression of amphibole to chlorite occurred and also biotite to chlorite, indicating greenschist-facies conditions associated with D3/D4 Laxfordian deformation events. In summary, our data agree with the subduction-accretionary prism tectonic model of Park *et al.* (2001) and add constraints on early metamorphic conditions through the sulfide deformation paragenesis where P reached 100 MPa prior to 150°C.

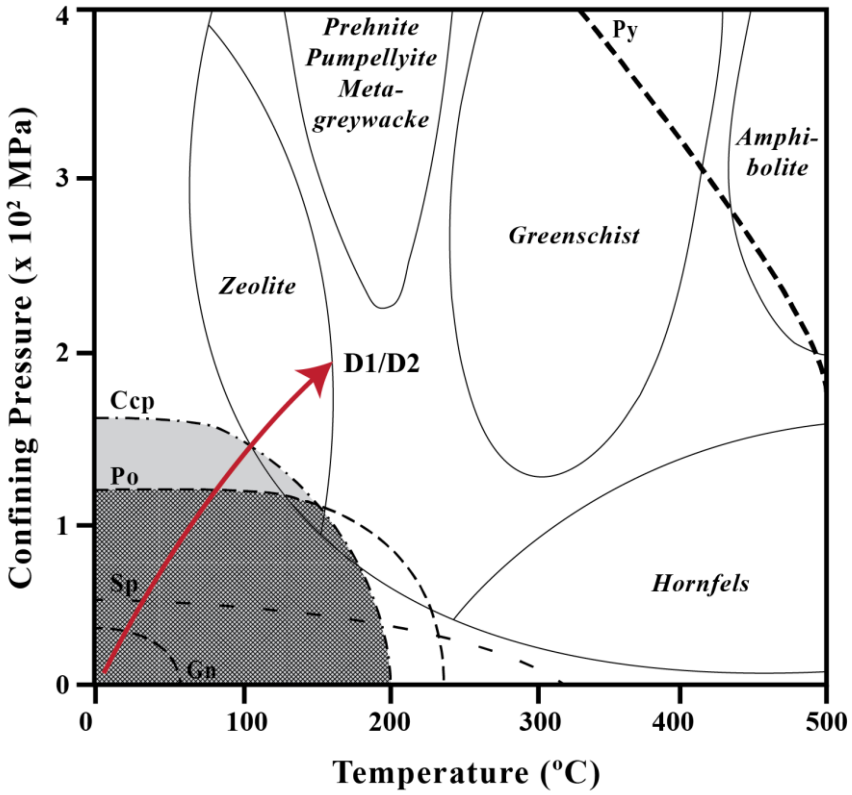

Figure 12: The brittle-ductile transitions of some common sulfides (from Marshal and Gilligan, 1987). Pyrrhotite was observed to mobilize first, followed by chalcopyrite and sphalerite. Shaded area outlines the path and minimum P-T conditions recorded by the sulfides during D1/D2 and the hashed area outlines maximum temperature and pressure during D3/D4. Ccp= chalcopyrite, Py= pyrite, Po= pyrrhotite, Sp= Sphalerite.

Implications for exploration of mafic-hosted VMS deposits in metamorphosed terranes to amphibolite facies

VMS deposits metamorphosed to the amphibolite facies are uncommon accounting for only 11 percent of known VMS deposits (Mosier *et al.*, 2009). In unmetamorposed environment, the primary alteration below the main massive sulfide consists of a zone of Mg- or Fe-rich chlorite proximal to the main upflow zone surrounded by a zone of distal white mica (Franklin *et al*., 2005; Galley *et al.*, 2007; Piercey, 2009; Hannington, 2014). Geochemically, these zones are associated with an increase in aluminous minerals relative to the host rock due to intense hydrothermal leaching of alkalis under acidic high fluid/rock conditions (e.g., Galley *et al.*, 2007; Dusel-Bacon, 2010). During metamorphism, the primary alteration mineral assemblage changes to aluminous minerals (garnet, chloritoid, staurolite, kyanite/andalusite/sillimanite and cordierite), orthorhombic Mg-Fe-Mn amphiboles and gahnite (zincian spinel) (e.g., Nesbitt and Kelly, 1980; Corriveau and Spry, 2014; Hollis et al., 2019). The final metamorphic assemblage depends on the peak metamorphic grade and the original composition of the host rock and alteration zone. At the Kerry Road deposit, no Al-rich phases, gahnite or orthoamphiboles were observed. Instead, calcic amphibole is the main alteration mineral. Its chemistry varies from actinolite in the mineralized zone to ferrotschermakite distal to mineralization (>150m) and defines a Mg-Si-rich halo surrounding the Kerry Road deposit. In addition to amphibole chemistry, whole-rock geochemistry records an enrichment in Si, Cu, Co, S, Zn, Fe, and Cd, and depletion in Al, Ti, V, Cr, Y and Zr, in regions proximal to the Kerry Road deposit (Fig. 8) associated with addition of sulfide and silica in silicate minerals related to mass gain during the hydrothermal alteration. Together, these proxies are typical of VMS deposits worldwide (e.g., Galley et al., 2007, Hannington, 2014, Cloutier *et al.*, 2017) and can be used to assess the proximity to

mineralization, not only for the LMG group, but for any metamorphosed VMS belts globally with similar metamorphic characteristics. In summary, despite the high amphibolite facies metamorphism recorded at the Kerry Road deposit, it is still possible to decipher the alteration surrounding the VMS deposit.

Conclusions

This study used a multi-faceted approach to analyze and assess one of Britain's oldest examples of VMS mineralization and its context to the regional geology. The Kerry Road deposit is a c. 2.0 Ga Paleoproterozoic VMS deposit, which formed in a submarine oceanic island arc setting from hydrothermal activity that sourced sulfur and base metals from sub seafloor tholeiitic basalt. The deposit was then deformed and metamorphosed during the 1.8-1.7 Ga Laxfordian orogeny. Sulfide textural relationships suggest a high-P low-T path that crossed 100 MPa before reaching 150°C during early deformation (D1/D2). Late Laxfordian deformation (D3/D4) is associated with brittle retrograde greenschist conditions with P-T of <1.2 MPa and <200°C). Our findings are compatible with the subduction-accretionary tectonic model of Park *et al.* (2001). Despite being exposed to amphibolite facies metamorphism, the original alteration halo associated with the Kerry Road deposit is preserved within amphibole crystal chemistry, with Mg- and Si-rich actinolites occurring with proximity to the Kerry Road deposit. In addition, whole rock geochemistry records a gradual Si, Cu, Co, S, Zn, Fe, and Cd enrichment, and Al, Ti, V, Cr, Y and Zr depletion, as the VMS system is approached. These proxies could be used for VMS exploration in highly metamorphosed mafic dominated terrane worldwide to vector toward mineralization.

Acknowledgments

We thank the British Geological Survey (BGS) for providing the opportunity to use their Keyworth Core Store facility and in particular, Eimear Deady and John Fletcher. We would also like to thank Donald Herd and Clare Crossan at the University of St Andrews, for their help and support towards this study, and Alison MacDonald and the NERC Isotope Community Support Facility at the Scottish Universities Environmental Research Centre for guidance and assistance on the conventional sulfur line. Steve Hollis and Mike Gadd are thanked for their constructive criticism and reviews of the manuscript.

References

Baker, T, Prave, AR, and Spencer, C (2019) 1.99 Ga Mafic Magmatism in the Rona terrane of the Lewisian Gneiss Complex in Scotland. Precambrian Research, v. 329, pp. 224–231.

Barrett, T.J., MacLean, W.H., and Areback, H. (2005) The Paleoproterozoic Kristineberg VMS deposit, Skellefte district, northern Sweden. Part II: chemostratigraphy and alteration. Mineralium Deposita, v. 40, pp. 368–395.

Barrie, CT and Hannington, MD (1999) Introduction: Classification of VMS deposits based on host rock composition, in Barrie, CT and Hannington, MD, eds., Volcanic-Associated Massive Sulfide Deposits: Processes and Examples in Modern and Ancient Settings: Reviews in Economic Geology, v. 8, pp. 2–10.

Bhattacharjee, CC (1968) The structural history of the Lewisian rocks north-west of Loch Tollie, Ross-shire, Scotland. Scottish Journal of Geology, v. 4, pp. 235–64.

Blättler, CL, Claire, MW, Prave, AR, Kirsimäe, K, Higgins, JA, Medvedev, PV, Romashkin, AE, Rychanchik, DV, Zerkle, AL, Paiste, K, Kreitsmann, T, Millar, IL, Hayles, JA, Bao,

H, Turchyn, AV, Warke, MR, and Lepland, A (2018) Two-billion-year-old evaporites capture Earth's great oxidation. Science, v. 360, no. 6386, pp. 320–323.

Cloutier, J, Piercey, SJ, Lode, S, Vande Guchte, M, and Copeland, D (2017) Lithostratigraphic and structural reconstruction of the Zn-Pb-Cu-Ag-Au Lemarchant volcanogenic massive sulphide (VMS) deposit, Tally Pond group, central Newfoundland, Canada. Ore Geology Reviews, v. 84, pp. 154–173.

Cloutier, J, Piercey, SJ, Layne, G, Heslop, J, Hussey, A, and Piercey, A (2015) Styles, Textural Evolution, and Sulfur Isotope Systematics of Cu-Rich Sulfides from the Cambrian Whalesback Volcanogenic Massive Sulfide Deposit, Central Newfoundland, Canada. Economic Geology, v. 110, no. 5, pp. 1215–1234.

Coates, J, Shaw, M, Gunn, A, Rollin, K, and Fortey, N (1997) Mineral Exploration in Lewisian supracrustal and basic rocks of the Scottish Highlands and Islands. Mineral Reconnaissance Programme Report. Keyworth, Nottingham: British Geological Survey. No.146, 91 pp.

Colman, T and Cooper, D (2000). Exploration for metalliferous and related minerals in Britain: A Guide. 2nd ed. Keyworth, Nottingham: British Geological Survey, 78 pp.

Cook, NJ and Hoefs, J (1997) Sulphur isotope characteristics of metamorphosed Cu-(Zn) volcanogenic massive sulphide deposits in the Norwegian Caledonides. Chemical Geology, v. 135, pp. 307–324.

Cook NJ and Marshall, B (2004) Metamorphic processes in ore formation and transformation. A thematic series of papers. Ore Geology Reviews, v. 24, pp. 169–171.

453 Cloutier, J., Piercey, S.J., Lode, S., Vande Guchte, M. and Copeland D.A. (2017)
454 Lithostratigraphic and structural reconstruction of the Zn-Pb-Cu-Ag-Au Lemarchant
455 volcanogenic massive sulphide (VMS) deposit, Tally Pond group, central Newfoundland,
456 Canada. Ore Geology Reviews, v. 84, pp. 154-173.

457 Corriveau, L and Spry, P (2014) Metamorphosed Hydrothermal Ore Deposits. Elsevier Ltd.,
458 (Treatise on Geochemistry 2nd Edition), pp.175–194.

459 Coward, MP (1990) Shear zones at the Laxfordian front, NW Scotland, and their significance
460 in the interpretation of lower crustal structure. Journal of the Geological Society, London,
461 v. 147, pp. 279–86.

462 Cox, S.F., 1987, Flow mechanisms in sulphide mineral. Ore Geology Reviews, v. 2, pp. 133–
463 171.

464 Davies, FB (1978) Progressive simple shear deformation of the Laxford shear zone, Sutherland.
465 Proceedings of the Geologists' Association 89, pp. 177–96.

466 Droop, GTR, Fernandes, LAD, and Shaw, S (1999) Laxfordian metamorphic conditions of the
467 Palaeoproterozoic Loch Maree Group, Lewisian Complex, NW Scotland. Scottish Journal
468 of Geology, v. 35, pp. 31–50.

469 Dusel-Bacon, C., Aleinikoff, J.N., Premo, W.R., Paradis, S., and Lohr-Schmidt, I. (2010)
470 Tectonic setting and metallogenesis of volcanogenic massive-sulfide deposits in the
471 Bonnifield mining district, northern Alaska Range. In Gough, L.P., and Day, W.C., eds.,
472 Recent U.S. Geological Survey studies in the Tintina gold province Alaska, U.S.A., and
473 Yukon, Canada – Summary results of a five-year project. U.S. Geological Survey
474 Scientific Investigations Report 2007-5289-B, pp. B1–B8.

475 Duuring, P., Hassan, L., Zelic, M., and Gessner, K. (2016) Geochemical and spectral footprint
476 of metamorphosed and deformed VMS-style mineralization in the Quinns District, Yilgarn
477 Craton, Western Australia. Economic Geology, v. 111, pp. 1411–1438.

478 Floyd, PA, Winchester, JA, and Park, RG (1989) Geochemistry and tectonic setting of
479 Lewisian clastic metasediments from the Early Proterozoic Loch Maree Group of Gairloch
480 NW Scotland. Precambrian Research, v. 45, pp. 203–214.

481 Franklin, JM, Gibson, HL, Jonasson, IR, and Galley, AG (2005) Volcanogenic Massive Sulfide
482 Deposits, in Hedenquist, JW, Thompson, JFH, Goldfarb, RJ, and Richards, JP, eds.,
483 Economic Geology 100th Anniversary Volume: The Economic Geology Publishing
484 Company, pp. 523–560.

485 Galley, A, Hannington, M, and Jonasson, J (2007) Volcanogenic Massive Sulphide Deposits.
486 Geological Association of Canada, Mineral Deposits Division, Special Publication. no. 5,
487 pp. 141–161.

488 Hannington, MD (2014) Volcanogenic Massive Sulfide Deposits, in Holland, HD and
489 Turekian, KK, eds., Treatise on geochemistry (second edition): Oxford, Elsevier, pp. 463–
490 488.

491 Hollis, S., Podmore, D., James, M., Menuge J.F., Doran, A.L., Yeats, C.J., and Wyche, S.
492 (2019) VHMS mineralization at Erayinia in the Eastern Goldfields superterrane: Geology
493 and geochemistry of the metamorphosed King Zn deposit. Australian Journal of Earth
494 Sciences, v. 66, n. 2, pp. 153–181.

495 Johnson, YA, Park, RG, and Winchester, JA (1987) Geochemistry, petrogenesis and tectonic
496 significance of the early Proterozoic Loch Maree Group amphibolites of the Lewisian

497 Complex, NW Scotland. In: Pharaoh, TC, Beckinsale, RD, and Rickard, D, eds.,
498 Geochemistry and Mineralization of Proterozoic Volcanic Suites. Geological Society of
499 London Special Publication, v. 33, pp. 255–269.

500 Jones, E, Rice, C, and Tweedie, J (1987) Lower Proterozoic stratiform sulphide deposits in
501 Loch Maree Group, Gairloch Northwest Scotland. The Institute of Mining and Metallurgy,
502 v. 96, pp. 128–140.

503 Large, RR (1977) Chemical evolution and zonation of massive sulfide deposits in volcanic
504 terrains. Economic Geology, v. 72, pp. 549–572.

505 Leake, BE, Woolley, AR, Arps, CES, Birch, WD, Gilbert, MC, Grice, JD, Hawthorne, FC,
506 Kato, A, Kisch, HJ, Krivovichev, VG, Linthout, K, Laird, J, Mandarino, JA, Maresch,
507 WV, Nickel, EH, Rock, NMS, Schumacher, JC, Smith, DC, Stephenson, NCN, Ungaretti,
508 L, Whittaker, EJW, Youzhi, G (1997) Nomenclature of amphiboles: Report of the
509 Subcommittee on Amphiboles of the International Mineralogical Association,
510 Commission on New Minerals and Mineral Names. European Journal of Mineralogy, v. 9,
511 pp. 623–651.

512 MacLean, WH (1988) Rare earth element mobility at constant inter-REE ratios in the alteration
513 zone at the Phelps Dodge massive sulphide deposit, Matagami, Quebec. Mineralium
514 Deposita, v. 23, pp. 231–238.

515 Marshall, B and Gilligan, L (1987) An introduction to remobilization: Information from ore-
516 body geometry and experimental considerations. Ore Geology Reviews, v. 2, pp. 87–131.

517 Marshall, B and Gilligan, L (1989) Durchbewegung structure, piercement cusps, and
518 piercement veins in massive sulfide deposits: Formation and interpretation: Economic
519 Geology, v. 84, pp. 2311–2319.
520 Marshall, B and Gilligan, L (1993), Remobilization, syn-tectonic processes and massive
521 sulphide deposits: Ore Geology Reviews, v. 8, pp. 39–64.
522 Mathieu, L. (2018) Quantifying hydrothermal alteration: A review of methods. Geosciences,
523 v. 8, n. 245, 27 pp.
524 McClay, K.R., 1995, The geometries and kinematics of inverted fault systems: a review of
525 analogue model studies. *In:* Buchanan, J.G. and Buchanan, P.G. (eds.), Basin inversion.
526 Geological Society Special Publication, v. 88, p. 97–118.

527 McClay, K and Ellis, P (1983) Deformation and Recrystallization of Pyrite. Mineralogical
528 Magazine, v. 47, pp. 527–538.

529 Mosier, D.L., Berger, V.I, and Singer, D.A. (2009) Volcanogenic massive sulfide deposits of
530 the world – Database and grade and tonnage model. U.S. Geological Survey Scientific
531 Investigations Report 2009–1034. http://pubs.usgs.gov/of/2009/1034/

532 Nelson, J., 1997, The quiet counter-revolution: Structural control of syngenetic deposits.
533 Geoscience Canada, v. 24, no. 2, p. 91–98.

534 Nesbitt, B.E. and Kelly, W.C. (1980) Metamorphic zonation of sulfides, oxides, and graphite
535 in and around the orebodies at Ducktown, Tennessee. Economic Geology, v. 75, pp. 1010–
536 1021.

537 Ohmoto, H and Rye, RO (1979) Isotopes of sulfur and carbon, in Barnes, HL, ed., The
538 geochemistry of hydrothermal ore deposits. New York, Wiley Interscience, pp. 509–567.

539 Park, RG (1964) The structural history of the Lewisian rocks of Gairloch, Wester Ross,
540 Scotland. Quarterly Journal of the Geological Society, v. 120, no. 1-4, pp. 397–426.

541 Park, RG, Crane, A, and Niamatallah, M (1987) Early Proterozoic Structure and Kinematic
542 Evolution of the Southern Mainland Lewisian. In: Park, RG and Tarney, J , eds, Evolution
543 of the Lewisian and Comparable High Grade Terrains. Geological Society Special
544 Publication no. 27, pp. 139–151.

545 Park, RG, Tarney, J, and Connelly, J (2001) The Loch Maree Group: Palaeoproterozoic
546 subduction–accretion complex in the Lewisian of NW Scotland. Precambrian Research, v.
547 105, pp. 205–226.

548 Peach, BN, Horne, J, Clough, CT, Hinxman, LW, and Teall, JJH (1907) The Geological
549 Structure of the North-West Highlands of Scotland. Memoir of the Geological Survey of
550 Great Britain, 668 pp.

551 Pearce, JA (1996) A user's guide to basalt discrimination diagrams. In: Wyman, DA, ed., Trace
552 element geochemistry of volcanic rocks: Applications for massive sulfide exploration, v.
553 12. Geological Association of Canada, Short Course Notes., pp. 79–113.

554 Piercey, SJ (2011) The setting, style and role of magmatism in the formation of volcanogenic
555 massive sulphide deposits. Mineralium Deposita, v. 46, pp. 449–471.

556 Piercey, SJ (2010) An overview of petrochemistry in the regional exploration for volcanogenic
557 massive sulphide (VMS) deposits. Geochemistry: Exploration, Environment, Analysis, v.
558 10, pp. 1–18.

559 Piercey, SJ (2009) Lithogeochemistry of volcanic rocks associated with volcanogenic massive
560 sulphide deposits and applications to exploration. In: Cousens, B and Piercey, SJ, eds.,

561 Submarine Volcanism and Mineralization: Modern through Ancient. Geological
562 Association of Canada. Short Course 29-30 May 2008, Quebec City, Canada, pp. 15–40.

563 Robinson, BW and Kusakabe, M (1975) Quantitative preparation of SO_2 for $^{34}S/^{32}S$ analysis
564 from sulfides by combustion with cuprous oxide: Analytical Chemistry, v. 47, pp. 1179–
565 1181.

566 Ross, PS and Bedard, JH (2009) Magmatic affinity of modern and ancient subalkaline volcanic
567 rocks determined from trace-element discriminant diagrams. Canadian Journal of Earth
568 Sciences, v. 46, pp. 823–839.

569 Seal, II, RR (2006) Sulphur isotope geochemistry of sulfide minerals: Reviews in Mineralogy
570 and Geochemistry, v. 61, pp. 633–677.

571 Shervais, JW (1982) Ti-V plots and the petrogenesis of modern and ophiolitic lavas. Earth
572 Planetary Science Letter, v. 59, pp. 101–118.

573 Shihe, L and Park, R (1993) Reversals of movement sense in Lewisian brittle-ductile shear
574 zones at Gairloch, NW Scotland, in the context of Laxfordian kinematic history. Scottish
575 Journal of Geology, v. 29, no. 1, pp. 9–19.

576 Skauli, H, Boyce, AJ, and Fallick AE (1992) A sulphur isotope study of the Blaekvassli Zn-
577 Pb-Cu deposit, Nordland, North Norway. Mineralium Deposita, v. 27, pp. 284–292.

578 Spry, PG, Marshall, B, and Vokes, FM (2000) Metamorphosed and metamorphogenic ore
579 deposits. Reviews in Economic Geology, v. 11, pp. 310.

580 Swinden, H.S., 1991, Paleotectonic settings of volcanogenic massive sulphide deposits in the
581 Dunnage Zone, Newfoundland Appalachians. Canada Institute of Mining and
582 Metallurgy Bulletin, v. 84, p. 59–89.

583 Torssander, P., 1992, Sulfur isotope ratios of leg 126 igneous rocks: Proceed- ings of the Ocean
584 Drilling Program, Scientific Results, v. 126, p. 449–453.

585 Vokes, FM (2000) Ores and metamorphism: Introduction and historical perspectives. Reviews
586 in Economic Geology, v. 11, pp. 1–18.

587 Wheeler, J, Park, RG, Rollinson, HR, and Beach, A (2010) The Lewisian Complex: Insights
588 into deep crustal evolution. Geological Society, London, Special Publications. v. 335, pp.
589 51–79.

590 Whitehouse, MJ, Bridgwater, D, and Park, RG (1997) Detrital zircon ages from the Loch Maree
591 Group, Lewisian Complex, NW Scotland: confirmation of a Palaeoproterozoic Laurentia-
592 Fennoscandia connection. Terra Nova, v. 9, pp. 260–263.

593 Williams, P, Tomkinson, M, and Cattell, A (1985) Petrology and deformation of
594 metamorphosed volcanic-exhalative sediments in the Gairloch Schist Belt, N.W. Scotland.
595 Mineralium Deposita, v. 20, no. 4, pp. 302–308.

596 Winchester, JA and Floyd, PA (1977) Geochemical discrimination of different magma series
597 and their differentiation products using immobile elements. Chemical Geology, v. 20, pp.
598 325–343.
599

List of Figures

622 Figure 5: Photo of mineralized intervals at the Kerry Road deposit. A) Sample highlighting the
623 common mineralogy and sulfide remobilization textures observed. Gangue includes quartz,
624 ferroan dolomite and calcite (GBH18; 30m). (B) VMS sample 70033 from drill core GBH23
625 at a depth of 29.45-29.7 m. Both samples show a remobilization sequence wherein pyrrhotite
626 crosses the brittle/ductile boundary first followed by chalcopyrite and sphalerite. Pyrite has not
627 been remobilized and acted brittlely during deformation. Ccp= chalcopyrite, Py= pyrite, Po=
628 pyrrhotite.

629 Figure 6: Photographs of the different sulfide mineralization texture. A) Disseminated
630 mineralization showing isolated chalcopyrite aggregates in a matrix of silicates. Drill core
631 GBH15, 20.5-22.5 m. B) Vein-type mineralization exploiting an ultramylonite horizon,
632 displaying chalcopyrite veining and pyrite cubes. Veining engulfs euhedral pyrite and is not
633 influenced by mylonitic shearing suggesting that remobilization continued to occur after peak
634 mylonitic conditions. Drill core GBH31, 73.16-73.36 m. C) Sub-massive texture displaying
635 both chalcopyrite and pyrrhotite mineralization. Drill core GBH41, 109.2-112 m. D) Massive
636 texture with dominant chalcopyrite. Drill core GBH19, 25.3-27.2 m. E) Durchbewegung
637 texture; defined as a mixture of secondary tectonic origin composed of angular to rounded
638 clasts of one or more competent materials in a matrix of predominantly different incompetent
639 material (in this case pyrrhotite). Significant clast rotation has occurred through deformation
640 to form this round clast (Marshall and Gilligan, 1987). Note the calcite exploiting the contact
641 between the VMS mineralization and the amphibole schist. Drill core GBH19, 33.0-33.4 m.

642 Figure 7: Immobile element discrimination diagrams for distal amphibolite surrounding the
643 Kerry Road deposit (A) Zr/TiO_2-Nb/Y diagram (Winchester and Floyd, 1977) with modified
644 field boundaries of Pearce (1996). B) Zr-Y discriminating magma affinity with fields of Ross
645 and Bedard (2009) (C) V-Ti/1000 diagram with field boundaries of Shervais (1982) for mafic

646 rocks. (D) Zr-Nb diagram of Piercey (2009) discriminating juvenile environments from
647 evolved environments. Low Ti-IAT Bon= low titanium-island-arc tholeiites and boninites,
648 IAT=island-arc tholeiites, MORB/BAB= mid-ocean ridge basalts/back-arc basalts.

649 Figure 8: Major and trace element A) enrichment and B) depletion associated with whole-rock
650 geochemical analysis along the Kerry Road deposit transect. Sample 2C is from the Kerry Road
651 VMS deposit; other samples are all associated with amphibolite host rock.

652 Figure 9: Isocon diagram (after Grant, 2005) illustrating the whole-rock chemical changes
653 between unmineralized and mineralized amphibolite. Major elements are in wt% and trace
654 elements in ppm.

655 Figure 10: Chemistry of amphibole at the Kerry Road area derived from microprobe analyses.
656 Amphibole chemistry changes from ferrotschermakite in distal samples (70060 and DD/16/04)
657 to actinolite in proximal samples (1A and 70027). This change highlights a progressive
658 enrichment in Si and Mg as the Kerry Road deposit is approached. Classification of calcic
659 amphiboles fields modified from Leake *et al.* (1997).

660 Figure 11: Sulfur isotope analysis (n=21) from the Kerry Road Deposit. The majority of the
661 samples are near 0 ‰ and reflect a basaltic source for the sulfur found in the base metal
662 sulfides.

663 Figure 12: The brittle-ductile transitions of some common sulfides (from Marshal and
664 Gilligan, 1987). Pyrrhotite was observed to mobilize first, followed by chalcopyrite and
665 sphalerite. Shaded area outlines the path and minimum P-T conditions recorded by the
666 sulfides during D1/D2 and the hashed area outlines maximum temperature and pressure
667 during D3/D4. Ccp= chalcopyrite, Py= pyrite, Po= pyrrhotite, Sp= Sphalerite.

668

669 **List of Tables**

674

675

676

Table 1. Whole-rock XRF results for the Kerry Road samples.

Sample name	Al %	Si %	P %	S %	K %	Ca %	Ti %	Mn %	Fe %	V ppm	Cr ppm	Co ppm	Ni ppm	Cu ppm	Zn ppm	As ppm	Rb ppm	Sr ppm	Y ppm
70023	0.38	10.64	<DL	29.70	0.02	6.54	0.010	0.067	38.94	18.1	297.2	593	163.2	3329	22570	<DL	17.9	6.9	13.6
70027	0.30	23.13	<DL	19.06	0.01	4.10	0.010	0.068	19.54	29.7	74	811	134.3	38180	6629	4.7	7.9	24	6.9
70033	0.26	0.20	<DL	14.15	0.01	16.98	0.001	0.168	16.5	43.8	57.5	450	10	2962	53200	22.5	6.4	19	25.9
70040	0.44	2.39	<DL	28.91	0.01	12.15	0.010	0.089	25.8	40.3	24.5	611	12.6	3758	64480	124.6	9	11.5	25.7
70041	0.34	1.54	<DL	26.46	0.01	10.18	0.010	0.159	25.99	31.6	10.3	849	16.2	4746	40160	73.4	11.7	7.5	20.6
70058	0.28	7.01	<DL	20.21	0.02	7.18	0.010	0.140	24.9	19.3	2.9	420	74.7	21550	20840	<DL	9.5	5.3	14.6
A	7.38	18.97	0.132	0.17	0.02	1.60	0.347	0.096	9.207	321.2	224.6	81.6	91.6	175.7	494.9	<DL	3.6	11.3	30.1
B	6.98	19.23	0.130	0.20	0.03	1.13	0.301	0.027	8.278	249.2	60	54.1	46	197.7	107.7	<DL	4	2.7	24.2
C	0.11	28.05	<DL	6.34	0.01	0.08	0.004	0.018	12.78	12.8	5	1336	29.1	1345	250	6.4	9.1	2.1	3.8
D	7.12	16.52	0.117	0.12	0.03	1.33	0.418	0.223	13.85	312.7	35.4	65.1	44.6	281.2	403.5	<DL	5.8	21.5	24.8
E (DD/16/20)	6.72	17.52	0.115	0.21	0.01	1.32	0.429	0.108	11.64	330.9	36.3	70.6	58.3	176	147.8	<DL	5.3	12	31.2
DD/16/14	0.31	21.58	<DL	24.43	0.01	3.96	0.010	0.030	22.01	11.9	6	780	39	11290	28670	<DL	8.7	0.8	15.3
DD/16/22	0.18	33.43	<DL	19.37	0.01	0.26	0.010	0.024	18.48	3	8	1839	17.5	3799	1740	4.2	10.8	2.1	4.4

<DL: Below detection limit

677 678

Table 1. Whole-rock XRF results for the Kerry Road samples (continued).

Sample name	Zr ppm	Nb ppm	Mo ppm	Ag ppm	Cd ppm	Sn ppm	Ba ppm	La ppm	Ce ppm	Pb ppm	Th ppm	U ppm	Lithology
70023	<DL	18.4	29.3	<DL	58.8	11.1	<DL	8.2	7.2	32.5	<DL	6	VMS mineralisation ~30% sulphides dominantly Po
70027	<DL	8.6	16.6	<DL	23.7	2.6	<DL	6.9	7	<DL	<DL	4.2	VMS mineralisation 15-20% Po, Chal, Py
70033	<DL	9.6	27	<DL	100.6	4.5	<DL	7.9	6.7	194.2	<DL	5.9	VMS strong sulphide mineralisation 25-30%
70040	<DL	16.5	32.4	<DL	131.4	11	<DL	< 5	5.7	594.1	<DL	8.1	VMS breciated mineralisation
70041	<DL	9	18.1	<DL	87.4	9.3	<DL	7.7	5.3	82.3	<DL	4.9	VMS
70058	<DL	9	19.4	<DL	49.5	8.6	<DL	<DL	6.5	<DL	<DL	8.1	VMS 25% sulphide mineralisation
A	62.8	4	1.8	<DL	<DL	<DL	5.8	<DL	<DL	0.7	1.1	1.4	Amphibolite
B	35.2	3.1	0.8	2	<DL	<DL	6.1	<DL	<DL	0.7	<DL	1.2	Amphibolite
C	10.9	1.7	9.2	47.2	<DL	<DL	5.3	<DL	<DL	15.7	<DL	2.9	VMS (highly weathered)
D	56.9	2.9	2.6	2.5	<DL	<DL	10.5	<DL	<DL	<DL	1.8	<DL	Folded amphibolite with Qz
E (DD/16/20)	65.3	4.1	1.5	2.9	<DL	<DL	4.7	<DL	<DL	0.7	1.8	<DL	Amphibolite
DD/16/14	<DL	7.9	15.3	<DL	52.3	2.1	<DL	<DL	<DL	<DL	<DL	5.8	VMS
DD/16/22	13	4.1	9.1	10.2	7.3	<DL	<DL	<DL	6.4	7.7	4.3	2.3	VMS

uctural formula of analyzed amphibole phases from the Kerry Road area.

	Zone	SiO_2 (%)	TiO_2 (%)	Al_2O_3 (%)	Fe_2O_3 (%)	MnO (%)	MgO (%)	CaO (%)	Na_2O (%)	K_2O (%)	Total (wt%)	Amphibole Name	Mineral formula
6)	Intermediate	50.96	0.44	4.61	12.71	0.00	14.72	11.97	0.54	0.00	95.95	Actinolite	$Na_{0.16}Ca_{1.90}(Mg_{3.24}Fe_{1.41}Al_{0.34}Ti_{0.05})(Si_{7.53}Al_{0.47})(OH)_2$
6)	Intermediate	52.47	0.12	3.26	13.96	0.00	15.68	12.24	0.41	0.00	98.15	Actinolite	$Na_{0.12}Ca_{1.91}(Mg_{3.40}Fe_{1.53}Al_{0.18}Ti_{0.015})(Si_{7.62}Al_{0.38})(OH)_2$
6)	Intermediate	53.27	0.12	3.51	12.67	0.00	15.52	11.80	0.27	0.07	97.24	Actinolite	$(Na_{0.0816}K_{0.01})Ca_{1.83}(Mg_{3.36}Fe_{1.38}Al_{0.33}Ti_{0.01})(Si_{7.73}Al_{0.27})(OH)_2$
6)	Intermediate	53.42	0.14	2.72	12.87	0.00	15.84	12.13	0.30	0.06	97.48	Actinolite	$(Na_{0.08}K_{0.01})Ca_{1.89}(Mg_{3.43}Fe_{1.41}Al_{0.22}Ti_{0.02})(Si_{7.75}Al_{0.25})(OH)_2$
6)	Intermediate	53.70	0.02	3.90	12.15	0.00	15.85	12.12	0.51	0.00	98.23	Actinolite	$Na_{0.14}Ca_{1.86}(Mg_{3.38}Fe_{1.31}Al_{0.35})(Si_{7.69}Al_{0.31})(OH)_2$
6)	Intermediate	52.47	0.13	4.85	11.59	0.00	15.36	11.89	0.43	0.01	96.73	Actinolite	$Na_{0.12}Ca_{1.85}(Mg_{3.32}Fe_{1.27}Al_{0.44}Ti_{0.01})(Si_{7.61}Al_{0.39})(OH)_2$
6)	Intermediate	52.15	0.01	2.88	12.46	0.00	15.75	12.30	0.30	0.00	95.84	Actinolite	$Na_{0.08}Ca_{1.95}(Mg_{3.474}Fe_{1.38}Al_{0.20})(Si_{7.70}Al_{0.30})(OH)_2$
6)	Intermediate	44.79	0.25	12.15	14.39	0.00	10.63	11.70	1.02	0.05	94.98	Mg-hornblende	$(Na_{0.30}K_{0.01})Ca_{1.90}(Mg_{2.40}Fe_{1.64}Al_{0.96}Ti_{0.03})(Si_{6.79}Al_{1.21})(OH)_2$
6)	Intermediate	46.21	0.37	10.20	15.15	0.21	11.53	11.86	1.02	0.13	96.68	Mg-hornblende	$(Na_{0.30}K_{0.03})Ca_{1.90}(Mg_{2.57}Fe_{1.71}Mn_{0.03}Al_{0.72}Ti_{0.04})(Si_{6.92}Al_{1.08})(OH)_2$
6)	Intermediate	52.95	0.01	3.86	14.12	0.00	15.69	11.93	0.27	0.10	98.92	Actinolite	$(Na_{0.08}K_{0.02})Ca_{1.84}(Mg_{3.37}Fe_{1.53}Al_{0.27})(Si_{7.62}Al_{0.38})(OH)_2$
6)	*Intermediate*	*51.24*	*0.16*	*5.19*	*13.21*	*0.02*	*14.66*	*11.99*	*0.51*	*0.04*	*97.02*	*Actinolite*	$(Na_{0.15}K_{0.01})Ca_{1.88}(Mg_{3.19}Fe_{1.46}Al_{0.40}Ti_{0.02})(Si_{7.50}Al_{0.50})(OH)_2$
6)	Intermediate	46.00	0.21	10.35	15.30	0.00	11.66	11.41	1.11	0.00	96.04	Mg-hornblende	$Na_{0.32}Ca_{1.84}(Mg_{2.62}Fe_{1.73}Al_{0.76}Ti_{0.02})(Si_{6.92}Al_{1.08})(OH)_2$
6)	Intermediate	49.87	0.25	8.12	14.67	0.00	13.15	12.05	0.76	0.00	98.87	Mg-hornblende	$Na_{0.21}Ca_{1.87}(Mg_{2.84}Fe_{1.60}Al_{0.61}Ti_{0.03})(Si_{7.22}Al_{0.78})(OH)_2$
6)	Intermediate	51.18	0.16	6.26	12.97	0.00	14.16	11.75	0.53	0.04	97.04	Mg-hornblende	$(Na_{0.15}K_{0.01})Ca_{1.84}(Mg_{3.08}Fe_{1.42}Al_{0.54}Ti_{0.02})(Si_{7.47}Al_{0.53})(OH)_2$
6)	Intermediate	51.12	0.17	6.83	13.28	0.00	14.01	11.76	0.51	0.11	97.78	Mg-hornblende	$(Na_{0.14}K_{0.02})Ca_{1.83}(Mg_{3.03}Fe_{1.45}Al_{0.58}Ti_{0.02})(Si_{7.41}Al_{0.59})(OH)_2$
6)	Intermediate	47.44	0.21	11.43	16.48	0.00	11.50	11.88	1.03	0.04	100.00	Mg-hornblende	$(Na_{0.29}K_{0.01})Ca_{1.84}(Mg_{2.48}Fe_{1.80}Al_{0.83}Ti_{0.02})(Si_{6.88}Al_{1.22})(OH)_2$
6)	Intermediate	53.66	0.07	3.89	12.20	0.00	15.61	12.16	0.38	0.01	97.98	Actinolite	$Na_{0.11}Ca_{1.87}(Mg_{3.34}Fe_{1.32}Al_{0.36}Ti_{0.01})(Si_{7.71}Al_{0.29})(OH)_2$
6)	Intermediate	52.90	0.01	2.79	14.38	0.00	14.11	11.65	0.37	0.15	96.37	Actinolite	$(Na_{0.11}K_{0.03})Ca_{1.85}(Mg_{3.11}Fe_{1.60}Al_{0.31})(Si_{7.82}Al_{0.18})(OH)_2$
6)	Intermediate	43.26	0.25	14.85	16.37	0.00	9.57	11.72	1.33	0.12	97.46	Mg-hornblende	$(Na_{0.39}K_{0.02})Ca_{1.88}(Mg_{2.13}Fe_{1.84}Al_{1.10}Ti_{0.03})(Si_{6.48}Al_{1.52})(OH)_2$
6)	Intermediate	45.21	0.23	13.74	15.17	0.56	9.91	12.22	1.20	0.13	98.38	Mg-hornblende	$(Na_{0.34}K_{0.02})Ca_{1.93}(Mg_{2.18}Fe_{1.68}Mn_{0.07}Al_{1.05}Ti_{0.03})(Si_{6.66}Al_{1.34})(OH)_2$
6)	Intermediate	45.86	0.27	12.62	15.83	0.00	10.94	11.42	1.24	0.11	98.30	Mg-hornblende	$(Na_{0.35}K_{0.02})Ca_{1.80}(Mg_{2.40}Fe_{1.75}Al_{0.94}Ti_{0.03})(Si_{6.75}Al_{1.25})(OH)_2$
6)	*Intermediate*	*48.65*	*0.18*	*9.09*	*14.66*	*0.06*	*12.46*	*11.80*	*0.85*	*0.07*	*97.82*	*Mg-hornblende*	$(Na_{0.24}K_{0.01})Ca_{1.85}(Mg_{2.72}Fe_{1.62}Mn_{0.01}Al_{0.71}Ti_{0.02})(Si_{7.13}Al_{0.87})(OH)_2$
m)	Proximal	54.19	0.03	1.57	10.14	2.76	17.79	11.44	0.63	0.04	98.59	Actinolite	$(Na_{0.18}K_{0.01})Ca_{1.76}(Mg_{3.80}Fe_{1.09}Mn_{0.33}Al_{0.03})(Si_{7.76}Al_{0.24})(OH)_2$
m)	Proximal	56.79	0.00	0.84	9.37	0.00	19.01	11.66	0.47	0.00	98.15	Actinolite	$Na_{0.13}Ca_{1.76}(Mg_{3.99}Fe_{0.99}Al_{0.13})(Si_{7.99}Al_{0.01})(OH)_2$
m)	Proximal	56.04	0.00	0.98	8.99	0.00	18.33	11.60	0.54	0.05	96.52	Actinolite	$(Na_{0.15}K_{0.01})Ca_{1.78}(Mg_{3.91}Fe_{0.97}Al_{0.18})(Si_{8.01})(OH)_2$
m)	Proximal	54.06	0.00	1.59	12.23	0.00	16.77	11.53	0.71	0.05	96.94	Actinolite	$(Na_{0.20}K_{0.01})Ca_{1.80}(Mg_{3.64}Fe_{1.34}Al_{0.13})(Si_{7.86}Al_{0.14})(OH)_2$
m)	Proximal	53.68	0.00	1.91	10.33	0.15	17.31	11.10	0.72	0.04	95.24	Actinolite	$(Na_{0.20}K_{0.01})Ca_{1.80}(Mg_{3.78}Fe_{1.14}Mn_{0.02}Al_{0.19})(Si_{7.86}Al_{0.14})(OH)_2$
m)	*Proximal*	*54.95*	*0.01*	*1.38*	*10.21*	*0.58*	*17.84*	*11.47*	*0.61*	*0.04*	*97.09*	*Actinolite*	$(Na_{0.17}K_{0.01})Ca_{1.77}(Mg_{3.82}Fe_{1.11}Mn_{0.07}Al_{0.13})(Si_{7.90}Al_{0.10})(OH)_2$
2 m)	Proximal	55.84	0.00	1.85	11.17	0.00	17.30	11.06	0.65	0.06	97.94	Actinolite	$(Na_{0.18}K_{0.01})Ca_{1.69}(Mg_{3.67}Fe_{1.20}Al_{0.25})(Si_{7.94}Al_{0.06})(OH)_2$
2 m)	Proximal	55.59	0.00	0.96	9.65	0.00	18.67	11.44	0.60	0.05	96.96	Actinolite	$(Na_{0.17}K_{0.01})Ca_{1.75}(Mg_{3.98}Fe_{1.04}Al_{0.11})(Si_{7.95}Al_{0.05})(OH)_2$
2 m)	Proximal	54.06	0.02	2.09	11.47	0.00	17.29	11.41	0.97	0.07	97.37	Actinolite	$(Na_{0.27}K_{0.01})Ca_{1.76}(Mg_{3.72}Fe_{1.24}Al_{0.15})(Si_{7.80}Al_{0.20})(OH)_2$
2 m)	Proximal	54.15	0.00	1.20	10.15	0.00	17.38	11.76	0.45	0.02	95.12	Actinolite	$Na_{0.13}Ca_{1.85}(Mg_{3.80}Fe_{1.12}Al_{0.14})(Si_{7.93}Al_{0.07})(OH)_2$
2 m)	*Proximal*	*54.91*	*0.01*	*1.53*	*10.61*	*0.00*	*17.66*	*11.42*	*0.67*	*0.05*	*96.85*	*Actinolite*	$(Na_{0.19}K_{0.01})Ca_{1.76}(Mg_{3.79}Fe_{1.15}Al_{0.18})(Si_{7.91}Al_{0.09})(OH)_2$
5 m	Distal	40.70	0.30	15.59	22.96	0.38	5.41	10.12	1.88	0.36	97.70	Ferrotschermakite	$(Na_{0.57}K_{0.07})Ca_{1.68}(Mg_{1.25}Fe_{2.69}Mn_{0.05}Al_{1.18}Ti_{0.04})(Si_{6.33}Al_{1.67})(OH)_2$
5 m	Distal	40.53	0.32	15.79	21.99	0.00	5.40	10.40	1.60	0.34	96.37	Ferrotschermakite	$(Na_{0.16}K_{0.00})Ca_{1.74}(Mg_{1.26}Fe_{2.59}Al_{1.25}Ti_{0.04})(Si_{6.34}Al_{1.66})(OH)_2$
5 m	Distal	38.61	0.31	15.54	22.78	0.00	5.07	10.49	1.94	0.35	95.09	Ferrotschermakite	$(Na_{0.60}K_{0.07})Ca_{1.80}(Mg_{1.21}Fe_{2.75}Al_{1.14}Ti_{0.04})(Si_{6.20}Al_{1.80})(OH)_2$
5 m	Distal	41.95	0.31	15.19	21.75	0.59	5.72	10.46	1.50	0.35	97.82	Ferrotschermakite	$(Na_{0.45}K_{0.07})Ca_{1.72}(Mg_{1.31}Fe_{2.52}Mn_{0.08}Al_{1.21}Ti_{0.04})(Si_{6.45}Al_{1.55})(OH)_2$
5 m	Distal	40.72	0.26	16.07	22.81	0.73	5.34	10.23	1.72	0.43	98.30	Ferrotschermakite	$(Na_{0.52}K_{0.08})Ca_{1.69}(Mg_{1.23}Fe_{2.65}Mn_{0.10}Al_{1.22}Ti_{0.03})(Si_{6.29}Al_{1.71})(OH)_2$

Table 2. Chemical composition in wt% and structural formula of analyzed amphibole phases from the Kerry Road area (continued).

Sample	Coordinates	Zone	SiO_2 (%)	TiO_2 (%)	Al_2O_3 (%)	Fe_2O_3 (%)	MnO (%)	MgO (%)	CaO (%)	Na_2O (%)	K_2O (%)	Total (wt%)	Mineral formula	
70060_Core 8	GBH51 27.4-25.5 m	Distal	41.48	0.34	15.01	22.44	0.08	5.87	10.02	1.84	0.27	97.33	Ferrotschermakite	$(Na_{0.55}K_{0.05})Ca_{1.66}(Mg_{1.36}Fe_{2.62}Mn_{0.01}Al_{1.17}Ti_{0.04})(Si_{6.43}Al_{1.57})(OH)_2$
70060_Core 9	GBH51 27.4-25.5 m	Distal	38.44	0.21	14.87	22.63	0.40	4.90	10.15	1.77	0.31	93.69	Ferrotschermakite	$(Na_{0.56}K_{0.06})Ca_{1.77}(Mg_{1.19}Fe_{2.78}Mn_{0.05}Al_{1.13}Ti_{0.03})(Si_{6.27}Al_{1.73})(OH)_2$
70060_Core 10	GBH51 27.4-25.5 m	Distal	42.31	0.27	16.19	20.80	0.69	5.40	10.56	1.38	0.38	97.99	Ferrotschermakite	$(Na_{0.41}K_{0.07})Ca_{1.73}(Mg_{1.23}Fe_{2.39}Mn_{0.09}Al_{1.36}Ti_{0.03})(Si_{6.45}Al_{1.55})(OH)_2$
70060_Core average	*GBH51 27.4-25.5 m*	*Distal*	*40.59*	*0.29*	*15.53*	*22.27*	*0.36*	*5.39*	*10.30*	*1.70*	*0.35*	*96.79*	*Ferrotschermakite*	$(Na_{0.52}K_{0.07})Ca_{1.73}(Mg_{1.26}Fe_{2.63}Mn_{0.04}Al_{1.21}Ti_{0.03})(Si_{6.34}Al_{1.66})(OH)_2$
70060_Rim 1	GBH51 27.4-25.5 m	Distal	40.77	0.32	15.91	21.05	0.49	5.15	9.94	2.42	0.36	96.41	Ferrotschermakite	$(Na_{0.73}K_{0.07})Ca_{1.66}(Mg_{1.20}Fe_{2.47}Mn_{0.06}Al_{1.29}Ti_{0.04})(Si_{6.37}Al_{1.63})(OH)_2$
70060_Rim 2	GBH51 27.4-25.5 m	Distal	40.34	0.33	15.70	23.36	0.71	5.03	9.92	2.00	0.29	97.69	Ferrotschermakite	$(Na_{0.61}K_{0.06})Ca_{1.66}(Mg_{1.17}Fe_{2.74}Mn_{0.09}Al_{1.18}Ti_{0.04})(Si_{6.30}Al_{1.70})(OH)_2$
70060_Rim 3	GBH51 27.4-25.5 m	Distal	41.63	0.24	15.48	21.62	0.56	5.51	10.19	1.78	0.32	97.33	Ferrotschermakite	$(Na_{0.53}K_{0.06})Ca_{1.69}(Mg_{1.27}Fe_{2.51}Mn_{0.07}Al_{1.25}Ti_{0.03})(Si_{6.44}Al_{1.56})(OH)_2$
70060_Rim 4	GBH51 27.4-25.5 m	Distal	39.18	0.36	15.93	21.53	0.85	5.27	10.03	1.86	0.29	95.30	Ferrotschermakite	$(Na_{0.57}K_{0.06})Ca_{1.71}(Mg_{1.25}Fe_{2.58}Mn_{0.12}Al_{1.22}Ti_{0.04})(Si_{6.23}Al_{1.77})(OH)_2$
70060_Rim 5	GBH51 27.4-25.5 m	Distal	41.10	0.21	16.76	22.38	0.90	5.13	9.91	2.11	0.31	98.81	Ferrotschermakite	$(Na_{0.63}K_{0.06})Ca_{1.63}(Mg_{1.17}Fe_{2.58}Mn_{0.12}Al_{1.32}Ti_{0.02})(Si_{6.29}Al_{1.71})(OH)_2$
70060_Rim 7	GBH51 27.4-25.5 m	Distal	40.89	0.40	16.17	22.95	0.68	5.40	10.25	1.99	0.29	99.01	Ferrotschermakite	$(Na_{0.59}K_{0.06})Ca_{1.68}(Mg_{1.23}Fe_{2.65}Mn_{0.09}Al_{1.19}Ti_{0.05})(Si_{6.27}Al_{1.73})(OH)_2$
70060_Rim 8	GBH51 27.4-25.5 m	Distal	41.26	0.28	15.51	22.35	0.35	5.34	10.11	1.78	0.38	97.35	Ferrotschermakite	$(Na_{0.53}K_{0.08})Ca_{1.68}(Mg_{1.24}Fe_{2.61}Mn_{0.05}Al_{1.24}Ti_{0.03})(Si_{6.40}Al_{1.60})(OH)_2$
70060_Rim 9	GBH51 27.4-25.5 m	Distal	40.79	0.34	15.21	20.41	0.42	5.11	10.35	1.41	0.29	94.33	Ferrotschermakite	$(Na_{0.43}K_{0.06})Ca_{1.76}(Mg_{1.21}Fe_{2.44}Mn_{0.06}Al_{1.32}Ti_{0.04})(Si_{6.47}Al_{1.53})(OH)_2$
70060_Rim 10	GBH51 27.4-25.5 m	Distal	41.16	0.21	16.01	21.87	0.42	5.36	10.32	1.94	0.36	97.65	Ferrotschermakite	$(Na_{0.58}K_{0.07})Ca_{1.71}(Mg_{1.23}Fe_{2.54}Mn_{0.06}Al_{1.27}Ti_{0.02})(Si_{6.36}Al_{1.64})(OH)_2$
70060_Rim average	*GBH51 27.4-25.5 m*	*Distal*	*40.79*	*0.30*	*15.85*	*21.94*	*0.60*	*5.25*	*10.11*	*1.92*	*0.32*	*97.10*	*Ferrotschermakite*	$(Na_{0.58}K_{0.06})Ca_{1.69}(Mg_{1.22}Fe_{2.57}Mn_{0.08}Al_{1.25}Ti_{0.04})(Si_{6.35}Al_{1.65})(OH)_2$
DD.16.04_Core 1	(183790, 872707)	Distal	39.93	0.18	15.64	23.43	0.42	4.90	10.86	1.77	0.52	97.65	Ferrotschermakite	$(Na_{0.54}K_{0.10})Ca_{1.82}(Mg_{1.15}Fe_{2.76}Mn_{0.06}Al_{1.15}Ti_{0.02})(Si_{6.26}Al_{1.74})(OH)_2$
DD.16.04_Core 2	(183790, 872707)	Distal	40.55	0.22	15.77	23.04	0.55	5.33	11.02	1.79	0.45	98.71	Ferrotschermakite	$(Na_{0.54}K_{0.09})Ca_{1.82}(Mg_{2.68}Fe_{2.68}Mn_{0.07}Al_{1.14}Ti_{0.03})(Si_{6.26}Al_{1.74})(OH)_2$
DD.16.04_Core 3	(183790, 872707)	Distal	40.43	0.30	16.10	23.03	0.48	4.94	11.24	1.75	0.44	98.70	Ferrotschermakite	$(Na_{0.52}K_{0.09})Ca_{1.86}(Mg_{1.14}Fe_{2.68}Mn_{0.06}Al_{1.18}Ti_{0.03})(Si_{6.25}Al_{1.75})(OH)_2$
DD.16.04_Core 4	(183790, 872707)	Distal	39.19	0.30	15.52	23.53	0.48	5.09	11.01	1.80	0.55	97.48	Ferrotschermakite	$(Na_{0.55}K_{0.11})Ca_{1.86}(Mg_{1.20}Fe_{2.79}Mn_{0.06}Al_{1.06}Ti_{0.04})(Si_{6.18}Al_{1.82})(OH)_2$
DD.16.04_Core 5	(183790, 872707)	Distal	39.58	0.22	15.44	23.13	0.33	5.14	11.01	1.62	0.43	96.90	Ferrotschermakite	$(Na_{0.50}K_{0.09})Ca_{1.86}(Mg_{1.21}Fe_{2.76}Mn_{0.04}Al_{1.12}Ti_{0.03})(Si_{6.24}Al_{1.76})(OH)_2$
DD.16.04_Core 6	(183790, 872707)	Distal	40.09	0.27	16.18	23.00	0.00	4.78	10.63	1.63	0.48	97.06	Ferrotschermakite	$(Na_{0.49}K_{0.10})Ca_{1.78}(Mg_{1.12}Fe_{2.71}Al_{1.26}Ti_{0.03})(Si_{6.28}Al_{1.72})(OH)_2$
DD.16.04_Core 7	(183790, 872707)	Distal	40.68	0.21	16.11	22.09	0.67	5.63	9.76	1.25	0.33	96.72	Ferrotschermakite	$(Na_{0.38}K_{0.07})Ca_{1.63}(Mg_{1.31}Fe_{2.59}Mn_{0.09}Al_{1.30}Ti_{0.02})(Si_{6.34}Al_{1.66})(OH)_2$
DD.16.04_Core 8	(183790, 872707)	Distal	40.37	0.25	16.11	21.41	0.63	5.52	10.48	1.57	0.34	96.69	Ferrotschermakite	$(Na_{0.47}K_{0.07})Ca_{1.75}(Mg_{1.28}Fe_{2.51}Mn_{0.08}Al_{1.26}Ti_{0.03})(Si_{6.30}Al_{1.70})(OH)_2$
DD.16.04_Core 9	(183790, 872707)	Distal	39.38	0.33	15.98	22.24	0.65	5.43	10.62	1.56	0.38	96.58	Ferrotschermakite	$(Na_{0.48}K_{0.08})Ca_{1.79}(Mg_{1.21}Fe_{2.68}Mn_{0.06}Al_{1.19}Ti_{0.04})(Si_{6.20}Al_{1.80})(OH)_2$
DD.16.04_Core 11	(183790, 872707)	Distal	40.14	0.14	15.79	23.13	0.00	4.97	10.42	1.73	0.33	96.65	Ferrotschermakite	$(Na_{0.53}K_{0.07})Ca_{1.75}(Mg_{1.17}Fe_{2.74}Al_{1.24}Ti_{0.02})(Si_{6.31}Al_{1.69})(OH)_2$
DD.16.04_Core average	*(183790, 872707)*	*Distal*	*40.03*	*0.24*	*15.86*	*22.80*	*0.42*	*5.17*	*10.70*	*1.65*	*0.43*	*97.31*	*Ferrotschermakite*	$(Na_{0.50}K_{0.09})Ca_{1.79}(Mg_{1.21}Fe_{2.68}Mn_{0.06}Al_{1.19}Ti_{0.03})(Si_{6.26}Al_{1.74})(OH)_2$
DD.16.04_Rim 1	(183790, 872707)	Distal	39.56	0.35	15.60	22.88	0.57	5.60	10.65	1.86	0.39	97.46	Ferrotschermakite	$(Na_{0.57}K_{0.08})Ca_{1.79}(Mg_{1.31}Fe_{2.70}Mn_{0.08}Al_{1.08}Ti_{0.04})(Si_{6.20}Al_{1.80})(OH)_2$
DD.16.04_Rim 2	(183790, 872707)	Distal	40.85	0.08	16.27	21.67	0.77	5.43	11.10	1.60	0.38	98.15	Ferrotschermakite	$(Na_{0.48}K_{0.08})Ca_{1.83}(Mg_{1.25}Fe_{2.51}Mn_{0.10}Al_{1.25}si_{0.01})(Si_{6.29}Al_{1.71})(OH)_2$
DD.16.04_Rim 3	(183790, 872707)	Distal	40.37	0.29	16.13	22.58	0.41	5.36	10.77	1.97	0.42	98.30	Ferrotschermakite	$(Na_{0.59}K_{0.080})Ca_{1.78}(Mg_{1.23}Fe_{2.63}Mn_{0.05}Al_{1.18}Ti_{0.03})(Si_{6.24}Al_{1.76})(OH)_2$
DD.16.04_Rim 4	(183790, 872707)	Distal	40.12	0.32	15.94	22.87	0.70	5.47	10.95	1.88	0.39	98.63	Ferrotschermakite	$(Na_{0.56}K_{0.08})Ca_{1.81}(Mg_{1.26}Fe_{2.66}Mn_{0.09}Al_{1.11}Ti_{0.04})(Si_{6.21}Al_{1.79})(OH)_2$
DD.16.04_Rim 5	(183790, 872707)	Distal	39.04	0.47	15.73	22.71	0.76	5.46	10.46	1.81	0.39	96.83	Ferrotschermakite	$(Na_{0.55}K_{0.08})Ca_{1.77}(Mg_{1.29}Fe_{2.70}Mn_{0.10}Al_{1.09}Ti_{0.06})(Si_{6.16}Al_{1.84})(OH)_2$
DD.16.04_Rim 6	(183790, 872707)	Distal	40.31	0.23	16.29	23.09	0.68	5.21	10.41	1.83	0.42	98.46	Ferrotschermakite	$(Na_{0.55}K_{0.08})Ca_{1.72}(Mg_{1.20}Fe_{2.69}Mn_{0.09}Al_{1.21}Ti_{0.03})(Si_{6.24}Al_{1.76})(OH)_2$
DD.16.04_Rim 7	(183790, 872707)	Distal	40.56	0.33	15.61	22.60	0.62	5.43	10.11	1.48	0.29	97.04	Ferrotschermakite	$(Na_{0.45}K_{0.06})Ca_{1.69}(Mg_{1.26}Fe_{2.66}Mn_{0.08}Al_{1.21}Ti_{0.04})(Si_{6.33}Al_{1.67})(OH)_2$
DD.16.04_Rim 8	(183790, 872707)	Distal	39.66	0.25	15.74	22.03	0.38	5.61	10.39	1.58	0.23	95.86	Ferrotschermakite	$(Na_{0.48}K_{0.05})Ca_{1.76}(Mg_{1.32}Fe_{2.62}Mn_{0.05}Al_{1.20}Ti_{0.03})(Si_{6.26}Al_{1.74})(OH)_2$
DD.16.04_Rim 9	(183790, 872707)	Distal	39.61	0.27	16.04	21.12	0.33	5.65	10.50	1.72	0.29	95.53	Ferrotschermakite	$(Na_{0.53}K_{0.06})Ca_{1.78}(Mg_{1.33}Fe_{2.51}Mn_{0.04}Al_{1.24}Ti_{0.03})(Si_{6.25}Al_{1.75})(OH)_2$
DD.16.04_Rim 11	(183790, 872707)	Distal	41.25	0.28	16.67	20.81	0.64	5.83	10.62	1.31	0.31	97.71	Ferrotschermakite	$(Na_{0.39}K_{0.06})Ca_{1.74}(Mg_{1.33}Fe_{2.40}Mn_{0.08}Al_{1.33}Ti_{0.03})(Si_{6.32}Al_{1.68})(OH)_2$
DD.16.04_Rim average	*(183790, 872707)*	*Distal*	*40.13*	*0.29*	*16.00*	*22.24*	*0.59*	*5.50*	*10.59*	*1.70*	*0.35*	*97.40*	*Ferrotschermakite*	$(Na_{0.51}K_{0.07})Ca_{1.77}(Mg_{1.28}Fe_{2.61}Mn_{0.08}Al_{1.19}Ti_{0.03})(Si_{6.25}Al_{1.75})(OH)_2$

Table 3. Measured $\delta^{34}S_{VCDT}$ from sulfides from the Kerry Road area

SAMPLE	δ34S (‰)
Pyrrhotite:	
70023	0
70044	-0.8
70048	-0.5
70049	1.1
Pyrite:	
70033	0.8
70039	0.7
70041	1.2
70045	1
70049	1.8
70050	2.1
70051	1.2
70052	0.8
70053	0.7
70057	1.1
70058a	0.7
70058b	1
Field	0.8
Chalcopyrite:	
70023	0.7
70038	0.9
70046	0.3
70054	1.2

681